INTERNATIONAL JOURNAL OF AUTOMOTIVE AND MECHANICAL ENGINEERING
ISSN: 2229-8649 e-ISSN: 2180-1606
VOLUME 22, ISSUE 3, 2025, 12748 - 12777
DOI: https://doi.org/10.15282/ijame.22.3.2025.16.0973

RESEARCH ARTICLE

Adaptive PI-Based Control for Steering Torque Feedback in Steer-by-Wire Systems: A Physical Modeling Approach

M. A. Azizul[1,2], F. Ahmad[1]*, J. Karjanto[1], M. H. Md Isa[1], and N. Mohamed[2,3]

[1]Faculty of Mechanical Technology and Engineering, Universiti Teknikal Malaysia Melaka, 76100 Hang Tuah Jaya, Melaka, Malaysia
[2]Faculty of Engineering Technology, Universiti Tun Hussein Onn Malaysia, 84600 Panchor, Muar, Johor, Malaysia
[3]Vehicle Dynamic & Sustainable Development (VeDys) Focus Group, Universiti Tun Hussein Onn Malaysia, 84600 Panchor, Muar, Johor, Malaysia

ABSTRACT – Steering feel is a crucial factor in Steer-by-Wire (SbW) architecture, where achieving the desired physical feedback is essential for driver experience. This research proposes the application of an adaptive Proportional-Integral (PI)-based controller as a torque tracking algorithm to achieve the targeted steering feel. To support this, a 14-DOF vehicle dynamic model was developed and validated in order to provide the foundation for a torque tracking algorithm to generate steering feel at the steering wheel. In the process of steering feel development, the SbW model was developed using a physical modeling approach based on Newton's laws, where the steering torque felt by the driver at the wheel corresponds to the torque generated by the rack and pinion assembly. The adaptive tracking torque algorithm is implemented using two methods, which are adaptive PI-based (A-PI) and gain scheduling PI-based (GS-PI) methods. The performance of these controllers was verified by using types of input signals (step and sinusoidal wave) and validated through three vehicle dynamic tests based on the ISO standards, including Double Lane Change, Slalom, and J-Turn tests. The findings showed that the GS-PI controller exhibited significant performance compared to results from the CarSim software, which served as a benchmark. Furthermore, the results indicated that this controller was capable of effectively replicating the desired steering feel with approximately less than 2.5 mean absolute error (MAE). This research study offers a practical control strategy for realistic steering feedback and contributes valuable insight for future SbW development.

ARTICLE HISTORY
Received : 10th Mar. 2025
Revised : 20th July 2025
Accepted : 11th Aug. 2025
Published : 22nd Sept. 2025

KEYWORDS
Torque feedback control
Steer-by-Wire
Physical model technique
Adaptive PI control
Vehicle dynamic

1. INTRODUCTION

Boasting automotive technology that is anticipated to transform the transportation sector, autonomous vehicles represent an unparalleled revolution in integrating modern technology. One such innovation is the incorporation of sophisticated technologies in the automotive niche, where the Steer-by-Wire (SbW) systems play a critical role. Additionally, SbW is a key component in the evolution of self-driving technology [1]-[3], as it combines with advanced sensors, advanced algorithms, and real-time data processing to navigate and replace human cognitive decision-making during driving sessions. One of the capability test platforms for autonomous vehicles is the actively steered front wheel system (Active Front Steer) [4], while SbW systems offer a groundbreaking solution that provides superior flexibility and precision in optimizing vehicle dynamics.

The importance of SbW systems is particularly pronounced in electric vehicles (EVs) and autonomous vehicles (AVs). For EVs, SbW technology complements the architecture by reducing weight, enhancing energy efficiency, and simplifying the vehicle's design, all of which contribute to extended battery life and improved travel range [5]-[6]. In AVs, SbW systems play a critical role in enhancing control precision and facilitating smoother, computer-guided driving operations, which are essential for autonomous navigation [7]. Furthermore, the ability to customize the steering response based on driving mode or environmental conditions makes SbW a promising technology for enhancing safety and adaptability in these advanced vehicles.

Building on the innovation brought by SbW technology, this system is fundamentally different from conventional steering systems, which depend on a mechanical link between the steering wheel and the wheels. Typically, conventional steering systems rely on a rack-and-pinion and steering column mechanism to establish the driver's confidence through the steering wheel feel developed from mechanical contact between the rack-and-pinion assembly and steering column assembly. This mechanical setup allows drivers to sense road conditions and adjust their steering input accordingly, which is crucial for vehicle control and stability. In contrast, the SbW architecture replaces this mechanical link with electronic signals, opening up possibilities for advanced steering customization and integration with other autonomous driving features.

Unfortunately, this advanced technology lacks responsive steering feel due to the absence of direct mechanical contact, which traditionally provides drivers with essential feedback on road texture, vehicle dynamics, and traction [8]-[9].

*CORRESPONDING AUTHOR | F. Ahmad | ✉ fauzi.ahmad@utem.edu.my

Steering feel is a fundamental aspect of any vehicle's handling characteristics, as it provides drivers or users with critical information regarding vehicle behavior and the characteristics of tire contact. This missing connection can lead to a reduction in driver confidence level, making it necessary to develop comprehensive controllers in SbW systems to stimulate a realistic and intuitive steering feel that at least meets the expectations of traditional steering experiences.

For the past several years, research has focused on understanding vehicle steering feel, aiming to replace the traditional steering mechanism with the SbW system. Steering feel development can be divided into two (2) approaches: physical modeling and data-driven methods. Physical modeling refers to the development of steering feel based on Newton's laws, requiring extensive knowledge of the contact interactions between linkages and the system's structural and dynamic characteristics. This approach has been dominant in recent years and necessitates a deep understanding of the interactions between components, from the steering wheel assembly to the road dynamic contact. However, steering systems are not governed solely by physical interactions; they also exhibit inherent characteristics such as compliance, damping, inertia, friction, and hysteresis. These properties may introduce significant challenges in accurately modeling the steering feel.

This method is based on fundamental physics and dynamics, allowing researchers to understand the underlying mechanics that govern steering behavior. In addition, the researchers can assess how the system would behave under various conditions, such as different road surface friction levels, wheel types, external wind disturbances, and varying steering inputs. Numerous studies have been conducted on developing steering feel in SbW systems using various approaches. These include designing mathematical equations based on dynamic forces generated by the wheels and assisting forces that mimic hydraulic power steering [10], creating mathematical formulations for a torque model based on tire-road contact [11]-[12], and formulating torque equations based on rack displacement changes in the rack and pinion assembly [13]-[16].

Balachandran and Gerdes [17] highlighted that the physical modeling method is an appropriate method for creating a realistic and tunable steering feel. Moreover, this method can be used to predict steering behavior under various driving conditions. The physical model is grounded in real-world physical laws that provide predictive insight into how the steering feels will evolve in different scenarios. Additionally, this model can be customized to accurately represent different vehicle types and steering mechanisms. In other words, researchers can directly control how the steering feels. The model can also manipulate parameters to simulate how changes in the suspension system, tire type, or vehicle load will affect steering feedback. The primary advantage of this approach is that it allows researchers to trace the origin of any steering behavior back to fundamental physical processes, making it easier to debug and troubleshoot issues.

The data-driven method relies on data to build a model for predicting or designing the steering feel. In other words, it uses data collected from actuators, such as sensors or through real-time experiments, to develop and replicate the steering feel. This approach requires data from various sources, and in the case of developing the steering feel, it requires data on the steering feel under various vehicle body conditions. The quality and quantity of data play a significant role in the effectiveness of this method. Over the years, this method has gained popularity due to its precision and efficiency in producing accurate results. Many researchers have successfully implemented data-driven methods to develop steering feel in the SbW system. Additionally, this method facilitates the introduction of various advance controllers such as neural network (NN) [18]-[20], sliding mode control (SMC) [21], adaptive sliding mode control (A-SMC) [22] and model predictive control (MPC) [23], along with torque mapping technique [24]-[25]. One of the significant advantages of the data-driven approach is its ability to mine and analyze experimental data using appropriate methods for model training and abstraction, without requiring explicit knowledge of the system's physical behavior. With proper data, a data-driven model can also ease or solve the contradiction between model precision and computational efficiency, particularly in real-time applications.

However, a data-driven method requires a large amount of real-world data to model steering feel accurately. The model's performance depends on the quality and diversity of the data used. There is a possibility that the data may be limited in certain cases, biased, or not representative of all possible conditions, which could lead the model to perform poorly or fail to generalize to new situations. Furthermore, developing an effective data-driven model requires broad real-world data collection, often through test drives, simulations, or sensor data gathering. This process can be time-consuming, expensive, and may require testing across various environments and driving conditions. Additionally, the system may need to be retrained or reset periodically as new data is collected, adding to the complexity. Even though advanced controllers have been introduced that focus on selecting data and tailoring it to certain conditions, the risk of latency issues increases, which can cause the model to respond too slowly to changes in driving conditions or driver input. This may also limit the model's performance in certain hardware applications that require higher computational performance due to the larger datasets involved, especially when implementing advanced controllers for diverse driving conditions.

By comparing both approaches, there is a similarity in the current implementation methods at the simulation stage. The development of both approaches typically involves simulation using low-degree-of-freedom vehicle dynamic models and implementation through the Hardware-in-the-Loop System (HiLS) method, with only a limited number of studies incorporating real-world experiments. This raises concerns regarding the accuracy and precision of the results produced, since the models often neglect the effects of suspension and tire characteristics, which can impact the reliability and consistency of the findings. Table 1 presents a literature review on steering feedback implementation methods in SbW systems, as well as the controllers used to generate steering feel based on both physical modeling and data-driven methods.

Table 1. Summary of Control Methods for Path Tracking and Steering Feel in SbW Systems

Control Objective	PT Controller	Method Modelling SF	SF Controller	Vehicle model	Reference
PT & SF	P control	Physical model	Road feedback model	2-DOF	[26]
PT & SF	SAT	Physical model	TSMC	2-DOF	[27]
PT & SF	IMC	Physical model	SMC	2-DOF	[28]
PT & SF	PI control	Physical model	Admittance control	2-DOF	[29]
PT & SF	Position-based control	Physical model	Torque mapping	3-DOF	[30]
SF	-	Data-Driven	Neural Network	2-DOF	[31]
SF	PID	Data-Driven	Torque mapping	CarSim	[32]
SF	-	Physical model	Road feeling compensation control model	CarSim	[33]
PT & SF	PI	Data-Driven	Road Feel Torque model	CarSim	[9]
SF	-	Data-Driven	MPC & CNN	-	[23]
PT & SF	PID	Data-Driven	SMC	-	[34]
PT & SF	PI	Physical model	Road sense feedback motor control	CarSim	[35]
SF	-	Data-Driven	ANN & GPR	-	[20]
SF	-	Data-Driven	EPS control logic	-	[36]
PT & SF	PID/LQR/MPC/SMC	Physical model	PID/LQR/MPC/SMC	2-DOF	[37]
PT & SF	LBC	Physical model	PSO tuning	2-DOF	[38]
SF	-	Data-Driven	Road sense planning method	2-DOF	[39]
SF	-	Physical model	TSM	2-DOF	[40]

*PT and SF are the path tracking and steering feel, respectively

Over the previous decades, various strategies have been proposed to develop steering feel in SbW systems, including methods such as sliding mode control (SMC), model predictive control (MPC), particle swarm optimization (PSO), terminal sliding mode (TSM), linear quadratic regulator (LQR) and convolutional/artificial neural network (C/A-NN), as shown in Table 1. The results presented by these advanced controllers have shown significant success in replicating steering feel behavior. However, the implementation of these controllers faces challenges, particularly the need for high computational power [41], which complicates real-time applications and increases the costs of experimental setups. Additionally, these advanced controllers present limitations, such as complexity issues [42]-[43] and sensitivity in tuning [44]-[48]. Thus, the full potential of the advanced controller embedded in the SbW steering system cannot be fully exploited and verified.

Despite these challenges, controllers in the traditional control group, namely, PID-based, are well-suited for implementation in steering feel systems, as they offer straightforward feedback control, are easy to develop, and exhibit high potential for real-time hardware system applications. Generally, a PID controller can be implemented or applied in different modes (proportional only (P-mode), proportional and integral (PI mode), proportional and derivative (PD-mode), and proportional, integral, and derivative (PID mode)), depending on process requirements [49]-[50]. In addition, PID control is widely used to manage many processes in industrial applications. The PID controller performs well under certain conditions, however, its effectiveness is limited in some cases. To overcome these limitations, significant research has been dedicated to enhancing PID controllers through techniques such as self-tuning, auto-tuning, genetic tuning, and robust optimal tuning [51]-[54]. These advancements allow the conventional PID controller to evolve into an adaptive PID-based controller. They can offer higher performance, especially when compared to traditional PID controllers, as they are designed to maintain optimal performance across a wider range of conditions [55].

An adaptive PID-based controller is recognized as an emerging technology that has been proven to have better performance than traditional PID in several applications. This advanced controller is a transformation based on various tuning strategies for the classical PID controller. An adaptive PID-based controller is commonly used in robotic motor control applications [56]-[59] in order to track motor speed, path, or force characteristics. The control strategy is cost-effective, making it a preferred choice for feedback control systems and a widely adopted solution in the development of robust control systems. However, despite its advantages, the adaptive PID-based controller remains relatively unpopular among researchers focusing on steering feel behavior in SbW systems involving motor applications as actuators. This is largely because the majority of research concentrates on the significant results achieved by advanced control techniques, while the challenges associated with integrating these advanced controllers into hardware systems, such as tuning complexity, time constraint development, and difficulty customization, are frequently overlooked. Therefore, further

investigation into the implementation of an adaptive PID-based controller is recommended, as its inherent benefits present a promising opportunity for advancing the development of steering feel in SbW systems.

This study investigated the development of steering torque feedback in the SbW system using a 14-degree-of-freedom (14-DOF) vehicle dynamics model, comparing the steering feel performance against the validated CarSim vehicle dynamics software. The contributions of this technical paper can be summarized as follows:

Contribution 1: A novel SbW system model is proposed, integrated seamlessly into a full 14-DOF vehicle dynamic model through simulation techniques. This integration enables the visualization and analysis of the dynamic behavior and impact of the SbW system on vehicle performance.

Contribution 2: A novel steering feel torque model and controller were developed for the Steer-by-Wire (SbW) system, aiming to replicate and enhance the driver's tactile feedback with high precision and practical applicability. The model is based on a physical modeling approach and incorporates an online tuning PID-based controller to ensure both accuracy and computational efficiency. Designed with real-time implementation in mind, the controller demonstrates strong potential for seamless hardware integration, making it suitable for next-generation SbW systems. Rigorous simulation-based validation confirms the model's effectiveness in reproducing realistic steering feel under real-world driving conditions.

This technical paper is structured into five sections. It begins with an introduction, including a review of relevant previous work on SbW steering feel development methods and testing environments. Section two presents the mathematical modeling of a comprehensive full-vehicle dynamic model. Section three describes the design of the SbW system, which replaces the conventional steering mechanism, and details its integration with the 14-DOF vehicle model. This section also provides an in-depth explanation of the proposed controllers used within the SbW architecture, along with performance verification using various signal inputs as reference signals. The validation process is presented in section four, where the effectiveness of the proposed controller in achieving realistic steering feel was demonstrated through vehicle dynamic tests based on ISO standards. Lastly, the conclusion of this study is presented in the final section.

2. STEER-BY-WIRE ARCHITECTURE THROUGH 14-DOF VEHICLE DYNAMIC MODEL

2.1 Non-Linear Vehicle Dynamic Model

To investigate the steering characteristics of the vehicle, it is crucial to carefully design the driver executor to ensure a comprehensive and accurate representation of the entire steering control process. This includes considering the interaction between the driver's inputs and the vehicle's response, which is essential for understanding the overall steering dynamics. A non-linear 14 DOF vehicle dynamic model was used in this study. Generally, a full (14-DOF) vehicle dynamic model can visualize yaw motion, roll motion, pitch motion, and nonlinear effects stemming from changes in vehicle geometry. This non-linear dynamic model includes the ride model, handling model, weight transfer model, lateral and longitudinal tire slip model, and tire dynamic model. In this study, the Pacejka tire model, commonly known as the "Magic Formula" tire model, was also used to present combined-slip tire behaviour in the vehicle dynamic model.

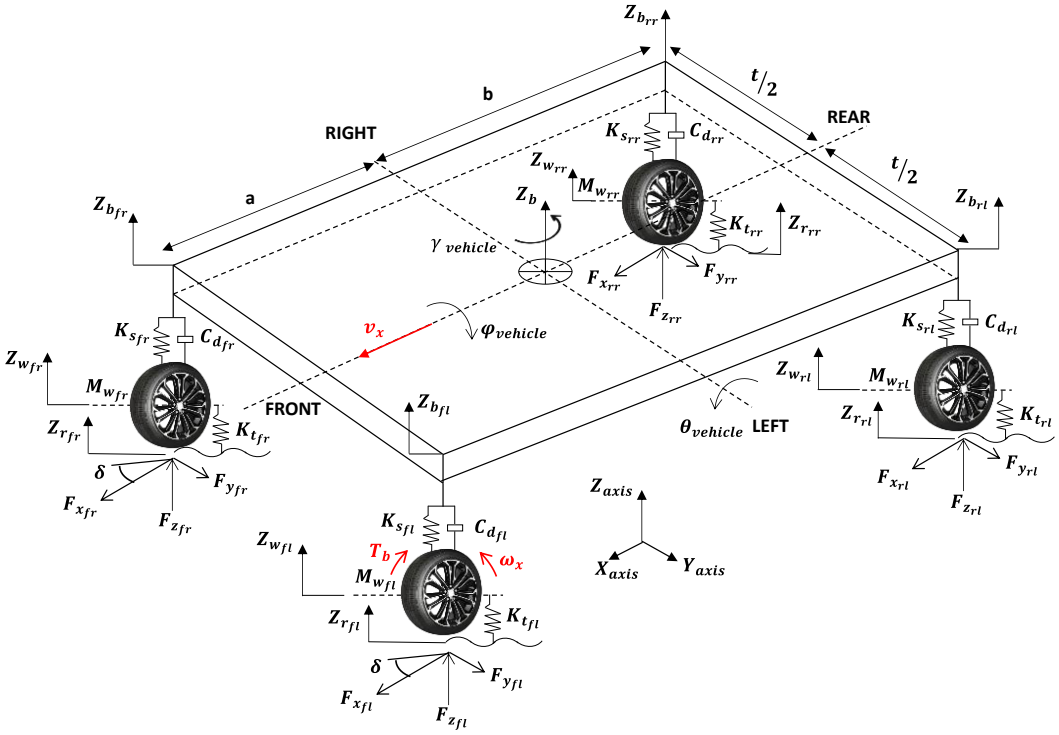

Figure 1. A 14-DOF vehicle dynamic model

In this study, several key assumptions were made. First, it was assumed that the suspension springs would not "top out" during maneuvering. Additionally, the vehicle was modeled as rigid, with the assumption that load transfer between points was 100% effective. The inner and outer steering angles were assumed to be equal throughout the simulation. The aerodynamic effects on the vehicle were neglected, and the road was considered flat, except for any potential disturbances. It was also assumed that the vehicle maintained constant contact with the ground during maneuvering, ensuring that all four tires remained in contact with the road surface. Finally, the coefficients and stiffness parameters in the vehicle dynamic model were presumed to remain constant throughout the simulation process. As illustrated in Figure 1, the 14-DOF vehicle model adeptly portrayed the dynamic characteristics across all vehicle axes.

- 6-DOF describes the free-body motion of the vehicle spring mass.
- 2-DOF for each of the four wheels represents the generalized position with respect to the body of the vehicle (derived from the suspension kinematics) and the longitudinal slip of the wheel.

The general equations governing the 14-DOF model are presented from equation (1) to equation (18), which were formulated by using Newton's Second Law. Ride model equations of motion in the full vehicle dynamic model are as follows:

$$M_b\ddot{Z}_b = F_{sfl} + F_{dfl} + F_{sfr} + F_{dfr} + F_{srl} + F_{drl} + F_{srr} + F_{drr} \tag{1}$$

where the spring stiffness, damper coefficient, and tire stiffness are defined as:

$$F_{si} = K_{si}(Z_{wi} - Z_{bi}) \tag{2}$$

$$F_{di} = C_{di}\left(\dot{Z}_{wi} - \dot{Z}_{bi}\right) \tag{3}$$

$$F_{ti} = K_{ti}(Z_{ri} - Z_{wi}) \tag{4}$$

The tire movement in the y-axis can be determined by:

$$M_w\ddot{Z}_{w_i} = F_{t_i} - F_{s_i} - F_{d_i} \tag{5}$$

The pitch effect of the vehicle is given by:

$$I_\theta\ddot{\theta} = (F_{srl} + F_{drl} + F_{srr} + F_{drr})(b) - \left(F_{sfl} + F_{dfl} + F_{sfr} + F_{dfr}\right)(a) \tag{6}$$

The roll effect of the vehicle is given by:

$$I_\varphi\ddot{\varphi} = \left(F_{sfl} + F_{dfl} + F_{srl} + F_{drl}\right)(t/2) - \left(F_{sfr} + F_{dfr} + F_{srr} + F_{drr}\right)(t/2) \tag{7}$$

The handling model equation of motion in this full vehicle dynamic model can be expressed as:

$$F_{x_{total}} = F_{xfl}\cos\delta - F_{yfl}\sin\delta + F_{xfr}\cos\delta - F_{yfr}\sin\delta + F_{xrl} + F_{xrr} \tag{8}$$

$$F_{y_{total}} = F_{xfl}\sin\delta + F_{yfl}\cos\delta + F_{xfr}\sin\delta - F_{yfr}\cos\delta + F_{yrl} + F_{yrr} \tag{9}$$

where the yaw effect of the vehicle is given by:

$$\begin{aligned} I_\gamma\ddot{\gamma} = {} & (t/2)\left\{\left(F_{xfl}\cos\delta\right) + \left(F_{yfl}\sin\delta\right) + \left(F_{xfr}\cos\delta\right) + \left(F_{yfr}\sin\delta\right)\right\} + \\ & (a)\left\{\left(\left(F_{xfl}\sin\delta\right) + \left(F_{yfl}\cos\delta\right) + \left(F_{xfr}\sin\delta\right) + F_{yfr}\cos\delta\right)\right\} + (b)\left\{F_{yrl} - F_{yrr}\right\} \end{aligned} \tag{10}$$

The weight transfer model can be formulated as follows:

$$F_{z_{,fi}} = \left(\frac{M_b g b - H_{CG} M_b a_x}{2(l)}\right) \tag{11}$$

$$F_{z_{,ri}} = \left(\frac{H_{CG} M_b a_x + M_b g a}{2(l)}\right) \tag{12}$$

The tire slip angle model can be expressed as follows:

$$\alpha_{fi} = \tan^{-1}\left[\frac{v_y + a\dot{r}}{v_x + \left(\frac{t}{2}\right)\dot{r}}\right] - \delta_f \tag{13}$$

$$\alpha_{ri} = \tan^{-1}\left[\frac{v_y - b\dot{r}}{v_x + \left(\frac{t}{2}\right)\dot{r}}\right] \tag{14}$$

Next, the longitudinal slip ratio of the front and rear tire can be represented as:

$$\sigma_{f/r} = \frac{\left(v_{tiref/r} - \omega_{f/r} R_w\right)}{\max\left(v_{xf/r}\,,\ \omega_{f/r} R_w\right)} \tag{15}$$

The tire dynamic model can be formulated as:

$$I_\omega \ddot{\omega}_{fi} \quad = T_{dfi} - T_{bfi} - T_{trac.fi} \tag{16}$$

$$I_\omega \ddot{\omega}_{ri} \quad = -(T_{bri} + T_{trac.ri}) \tag{17}$$

The common equation of motion for the Pacejka Tire model is given by:

$$F(x) = \quad D\cos\left(C\tan^{-1}\left(Bx - E(Bx - \tan^{-1}(Bx))\right)\right) \tag{18}$$

The symbols used in the development of the 14-DOF vehicle dynamic model are listed in Appendix A. Further information on the structure of the 14-DOF vehicle dynamic model can be found in [60], where the governing equations are thoroughly explained and discussed. This non-linear vehicle dynamic model was validated using certified vehicle dynamics software, CarSim software, with the results compared to actual vehicle dynamics tests conducted in accordance with ISO standards through simulation-based methods. Further details and explanations of the validation process, including graphical plots and root mean square (RMS) percentage error, are also provided in this technical paper.

2.2 Steer-by-Wire Architecture

In the context of modeling the SbW system, there are two (2) subsystems involved, which are the steering wheel model and the front wheel model. The steering wheel model in such a system consists of a steering wheel assembly, a motor shaft, and a feedback motor. The steering wheel assembly functions to detect the driver's input, such as steering angle or steering torque. These inputs are transmitted as an electrical signal through the shaft motor, while the feedback motor serves as the actuator to generate the force feedback to simulate the feel at the steering wheel. This sub-model describes the dynamic behavior of the steering wheel, steering column, and DC motor in both mechanical and electrical domains. Figure 2 illustrates the free-body diagram of the steering wheel model, which was developed based on Newton's law of motion.

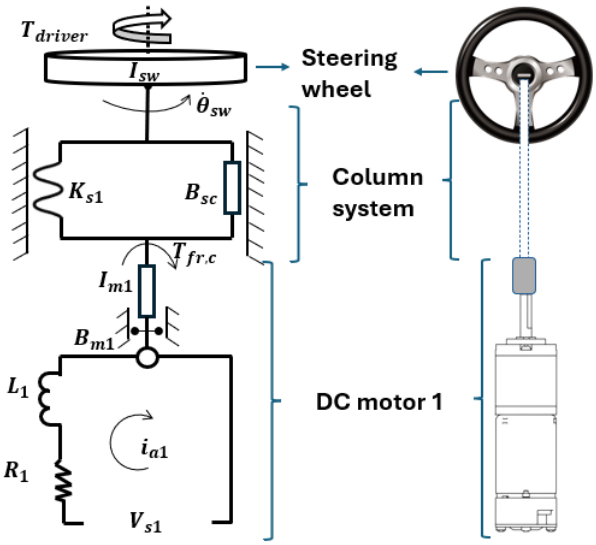

(a) (b)

Figure 2. The steering wheel assembly in SbW architecture: (a) free body diagram of steering wheel model [60], (b) steering wheel and column system in SbW system

To derive the steering wheel model, it is crucial to first understand the components involved and identify the relevant dynamics of the steering wheel model in the SbW system. The equation of motion for the steering wheel was derived based on Newton's 2nd law for rotational systems:

$$\sum \tau = \mathrm{I}\alpha \tag{19}$$

In this equation, the torque,τ represents the net torque acting on the body of the steering wheel assembly. To summarize, the moment of inertia of the steering wheel, I, multiplied by the angular acceleration, α, is equal to the total summation of torques acting on the steering wheel assembly, including the restoring torque, damping torque, friction torque, and the driver torque input. The torques generated by the steering column consist of the restoring torque, damping torque, and friction torque. The restoring torque can be expressed as:

$$\text{Restoring torque} \quad = K_{S1}(\theta_{sw} - \theta_{m1}) \tag{20}$$

Here, the restoring torque is associated with the stiffness coefficient (spring constant), which provides the return-to-center force felt by the driver. The relative angular displacement between the steering wheel, θ_{sw} and the motor, θ_{m1} is a fundamental aspect of the steering system, as it governs the feedback experienced by the driver.

The damping and friction torque can be defined as:

$$\text{Damping torque} \quad = B_{sc}\left(\dot{\theta}_{sw} - \dot{\theta}_{m1}\right) \tag{21}$$

$$\text{Friction torque} \quad = T_{fr,c} \tag{22}$$

where, the damping torque resists relative motion within the system. It dissipates energy, typically in the form of heat, and helps stabilize the system. Damping force prevents excessive oscillations or vibrations in the steering mechanism and contributes to the steering feel by ensuring smooth and controlled movements. The friction torque represents resistance due to mechanical friction in the steering column or motor bearings. It provides additional resistance to movement, further enhancing the overall steering feel. Based on Figure 2(a), the dynamic equation governing the steering wheel dynamics can be expressed as equation (23), which involves several torque components: restoring torque, damping torque, coupled damping torque, and motor torque.

$$\begin{aligned} \sum \tau = I\alpha = I_{sw}\ddot{\theta}_{sw} \\ \sum \tau \quad &= T_{driver} + T_{damping} + T_{spring} + T_{fr,c} \\ I_{sw}\ddot{\theta}_{sw} \quad &= \left(T_{driver} - B_{sc}\left(\dot{\theta}_{sw} - \dot{\theta}_{m1}\right) - K_{S1}(\theta_{sw} - \theta_{m1}) - T_{fr,c}\right) \end{aligned} \tag{23}$$

The damping torque opposes motion due to the motor speed, while the restoring torque resists displacement. The coupled damping torque opposes the relative motion between the motor and the steering wheel. Based on Figure 2(a), the dynamic equation governing the motor dynamics can be expressed as:

$$I_{m1}\ddot{\theta}_{m1} \quad = \left(T_{m1} - B_{m1}\dot{\theta}_{m1} - B_{sc}\left(\dot{\theta}_{m1} - \dot{\theta}_{sw}\right) - K_{S1}(\theta_{m1} - \theta_{sw})\right) \tag{24}$$

The electrical equation is formulated based on Kirchhoff's Voltage Law, where the motor's electric dynamic equation can be defined as:

$$V_{S1} \quad = \left(V_{inductor} + V_{motor\ resistance} + V_{emf}\right) \tag{25}$$

$$= \left(L_1 \frac{di_{a1}}{dt} + R_1 i_{a1} + k_e \dot{\theta}_{m1}\right) \tag{26}$$

The symbols and corresponding values used in the development of the steering wheel model are provided in Appendix B (Table B-1).

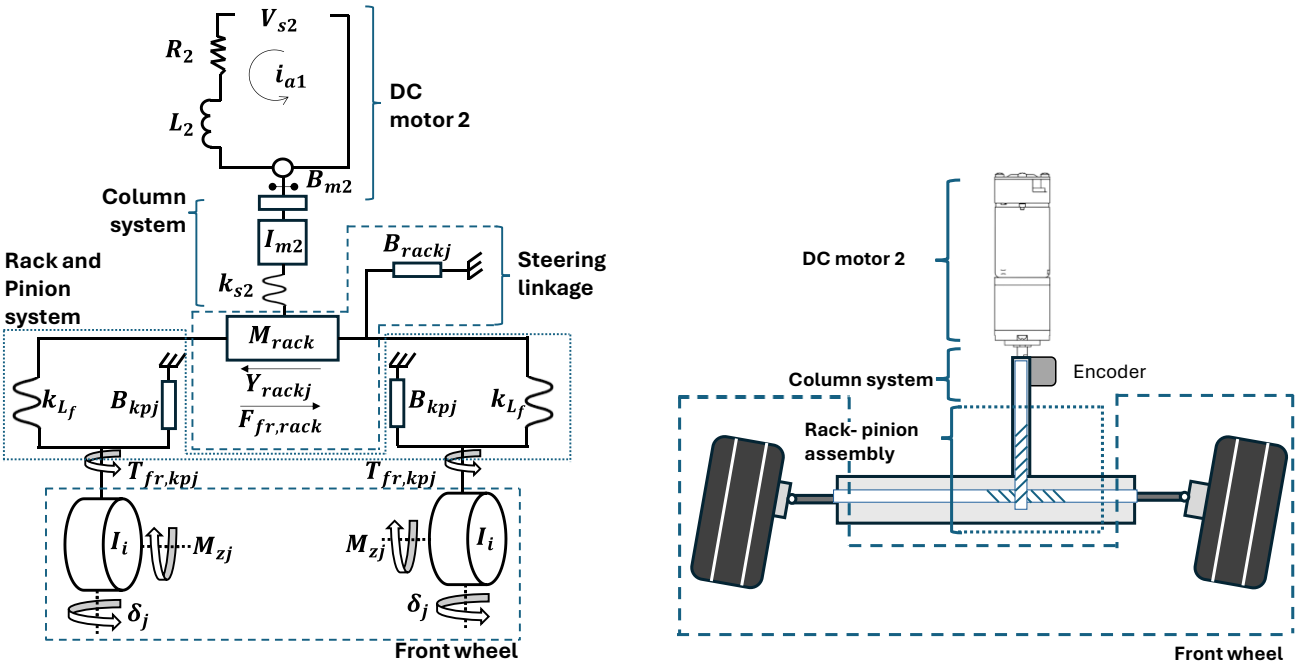

(a) (b)

Figure 3. The front wheel assembly in SbW architecture: (a) free body diagram of front wheel model [60], (b) steering wheel and column system in SbW

The front wheel model in the SbW system typically consists of several interconnected components: the front wheel itself, the rack and pinion assembly, steering linkage assembly, motor shaft, and steering motor (acting as an actuator). Crucial information from the steering wheel, such as the steering wheel angle, is captured by sensors and transmitted to the electric control module. The steering motor serves as an actuator, converting the electric signal from the electric control module into mechanical movement. The motor shaft guides for the rack and pinion assembly, which translates the steering wheel angle into the appropriate front wheel angle. This allows the driver to control the vehicle's direction without the need for a traditional mechanical linkage between the steering wheel and the wheels. The free body diagram of the front wheel model is shown in Figure 3(a), while the illustration of the front wheel assembly in the SbW system is shown in Figure 3(b).

To derive the equation of the front wheel model, it is necessary to identify the forces acting on the rack. These forces acting on the rack are explained below, from equation (27) to equation (38). The equation of motion for the rack displacement dynamic was derived using Newton's 2nd law for linear motion, and is defined as:

$$\sum F = ma \tag{27}$$

The spring force, resulting from the tire generating a lateral force based on its stiffness, is defined as:

$$F_{spring} = 2K_{L_f}\left(\frac{y_{rack_y}}{r_L} - \delta_F\right) \tag{28}$$

Additionally, there is a force acting due to motor 2 feedback through a stiffness mechanism, expressed as:

$$\begin{aligned} F_{motor2}\, r_P &= T_{motor2} \\ F_{motor2}\, r_P &= K_{S_2}\left(\frac{y_{rack_y}}{r_L} - \delta_F\right) \\ F_{motor2} &= \frac{K_{S_2}}{r_P}\left(\frac{y_{rack_y}}{r_L} - \delta_F\right) \end{aligned} \tag{29}$$

Here, the term $\frac{y_{rack_y}}{r_L}$ transforms the rack displacement into an equivalent steering angle (lever ratio). Also included is the friction force opposing the motion, and the rack damping force, which are expressed as:

$$F_{friction} = F_{fr,rackf} \tag{30}$$

$$F_{damping} = B_{rack}\, \dot{y}_{rack_f} \tag{31}$$

Thus, the equation of the dynamics of the rack can be expressed as:

$$\begin{aligned} \sum F = ma &= M_{rack}\ddot{y}_{rack_y} \\ \sum F = ma &= F_{spring} + F_{friction} + F_{damping} + F_{motor} \\ M_{rack}\ddot{y}_{rack_y} &= \left(-\frac{2K_{Lf}}{r_L}\left(\frac{y_{rack_y}}{r_L} - \delta_F\right) - F_{fr,rack_f} - B_{rack_f}\dot{y}_{rack_y} + \frac{K_{S2}}{r_P}\left(\theta_{m2} - \frac{y_{rack_y}}{r_P}\right)\right) \end{aligned} \tag{32}$$

At the front wheel steering axis, the rotational dynamics of the front wheel in the SbW system can be described as the sum of the torques about the kingpin axis. The torques involved include the spring torque, which represents the restoring force from the rack. This torque is proportional to the lateral stiffness and the difference between the steering angle and the rack-induced displacement, and can be expressed as:

$$T_{spring} = K_{L_f}\left(\delta_F - \frac{y_{rack_y}}{r_L}\right) \tag{33}$$

Another torque is the friction torque, which arises from the resistance at the kingpin opposing rotational motion. The damping torque, resulting from damping in the kingpin's rotation, contributes a torque proportional to angular velocity. Additionally, there is an external torque, which is the moment acting on the front wheel due to lateral forces on the tires. These torques are expressed as:

$$T_{friction} = T_{fr,kpf} \tag{34}$$

$$T_{damping} = B_{kp}\, \dot{\delta}_F \tag{35}$$

$$T_{external} = M_z \tag{36}$$

Thus, the equation for the rotational dynamics about the kingpin axis can be written as:

$$\sum \tau = I\alpha = I_f \ddot{\delta}_F \tag{37}$$

$$\sum \tau = I\alpha \quad = T_{spring} + T_{friction} + T_{damping} + T_{external}$$
$$I_f \ddot{\delta}_F \quad = \left(-K_{Lf}\left(\delta_F - \frac{y_{rack_y}}{r_L}\right) - T_{fr,kpf} - B_{kpf}\dot{\delta}_F - M_z\right)$$

The dynamic equation for motor 2 can be defined as:

$$I_{m2}\ddot{\theta}_{m2} \quad = \left(T_{m2} - B_{m2}\dot{\theta}_{m2} - K_{S2}\left(\theta_{m2} - \frac{y_{rack_y}}{r_P}\right)\right) \tag{38}$$

The symbols and corresponding values used in the development of the front wheel model are provided in Appendix B (Table B-2). Comprehensive details on the simulation validation of the SbW system and the experimental setup using the Hardware-in-the-Loops system (HiLs) method for validation purposes are provided in [60].

3. STEERING FEEDBACK CONTROL IN SbW SYSTEM

Steering feel refers to the torque or force feedback that the driver receives through the steering wheel, providing a sense of the vehicle's road behavior and handling characteristics. There are several methods or techniques to develop steering feel in the SbW system, which are explained in detail in section 1.0. One of the recognized approaches is the physical model technique, also known as the model-based approach, which relies on dynamic mathematical equations to describe the behavior of the steering system. This technique is based on physical laws, such as Newton's law of motion, and assumes that a comprehensive understanding of the system's characteristics is available.

In order to develop steering feedback control in the SbW system, various approaches have been proposed over the past few decades, particularly within the framework of the physical model technique used to describe steering feel. In the early stages, several researchers have focused on modeling the road model through mathematical equations. In other words, to develop steering feel, researchers adopted an approach where the movement of the tire on the vehicle could accurately reflect actual road conditions, which in turn affect the steering feel at the steering wheel. As a result, various design algorithms have been proposed to simulate both the road's feel and steering feel in the SbW system. The development of road models aims to investigate how various road conditions influence the feedback forces experienced by the driver, as well as to acquire information on the forces or torques occurring at the tire-road surface contact. This approach is illustrated in the research works by [9],[27],[35],[61]-[63], where a steering feedback model was developed by capturing tire-to-ground contact information using a low-order vehicle dynamic model. These studies presented several mathematical equations to describe the critical components involved in the front wheel assembly model, including the road feel control model, assisting torque model, self-aligning torque, and jacking torque model, in addition to the equations presented in subsection 2.2, which encompass the SbW model.

The contributions of researchers in this niche area have shown that the road model algorithms are highly effective, with results indicating a close replication of the steering feel generated by the system. Comparisons were made between the model outputs and validation results obtained from simulation tools, such as Carsim, as well as experimental data from HiLs testing. However, to ensure that the road model algorithms truly represent real-world tire conditions, the model must undergo precise validation to confirm their accuracy in reflecting actual road behavior. The validation methods and required equipment can be complex, expensive, and technically challenging. Consequently, questions remain as to whether such road models can reliably account for all potential driving scenarios when applied to simulate steering feel under various driving conditions.

Furthermore, several researchers have also adopted a hysteresis model approach to design steering feel in SbW systems, utilizing mathematical modeling to replicate and simulate realistic steering feedback. Specifically, the Bouc-Wen hysteresis model has been applied to characterize the torque response at the steering wheel, with its primary function being the emulation of nonlinearities and dynamic lag effects typically observed in conventional mechanical steering systems. The Bouc-Wen model is derived from a set of mathematical equations that capture the nonlinear, memory-dependent characteristics of steering feel. Key parameters within this model, including stiffness, damping, and shape factors, govern the torque response relative to the steering angle. These parameters can be fine-tuned and have been used to adjust the torque feedback curve [64], modify the inherent nonlinearities in the steering response [65]-[66], and customize the shape of the hysteresis loop [64],[67]-[68]. Additionally, this model allows for the integration of tire-road interaction dynamics [69] into the steering feel, thereby enhancing the realism of the feedback.

The contributions of these respective researchers have been instrumental in the development of hysteresis models in the SbW system, allowing for the adjustment of model parameters to achieve various steering characteristics. These adjustments can modify factors such as steering feedback softness with reduced resistance or create a smoother return-to-center feel, thus enhancing adaptability and driver responsiveness across a range of driving conditions. However, despite its flexibility and realism, the Bouc-Wen hysteresis model presents several challenges when it comes to hardware implementation. These challenges include high computational requirements for real-time processing, complex parameter tuning, and difficulties in accurately modeling tire-road interactions. Moreover, the need for sophisticated and expensive validation equipment further complicates the practical application of this model. As a result, these limitations hinder the reliability and scalability of the Bouc-Wen hysteresis model for use in the development of steering feel in SbW systems.

Aside from this, several researchers have also introduced alternative approaches to develop artificial steering feel in the SbW system. For instance, Irmer et al. [70] introduced a simplified model for the sub-systems of the steering wheel and front wheel assembly to replicate the steering feel. Simulation results from this study demonstrated that the reduced-order SbW model could replicate the performance of the traditional Electronic Power Steering (EPS) system. However, the control system exhibited limited robustness characteristics, particularly in response dynamic behaviour. Specifically, the model reduction may overlook key dynamic factors, which can impact the system's performance under real-world conditions.

Although various researchers have successfully generated steering feel and verified using certified simulation tools, the present methods exhibit several shortcomings: 1st, the complexity of the system arises from the numerous mathematical models involved in steering feel development, which leads to challenges in achieving accurate representation; 2nd, these mathematical models often require the simplification of certain parameters, which only meet the required conditions under specific scenarios; 3rd, the set of mathematical models requires validation with actual hardware; for example, to assess whether the torque at the front wheel or kingpin assembly contributes to the development of steering feel, it is necessary to install sensors to validate the torque value. This is a challenging task not only due to the complexity of the validation process, but also involves substantial financial costs.

Considering the factors mentioned above, this study focuses on replicating the torque flow of a traditional rack-and-pinion system within the SbW framework. Generally, for a conventional rack and pinion steering system, the torque experienced at the steering wheel is a result of multiple forces generated by the front wheel assembly, including kingpin torque, suspension linkages, wheel rotation, and dynamic road forces. These forces combine to produce a resultant force at the rack-and-pinion interface, which drives the steering angle of the wheels. In other words, the torque transmitted from the rack and pinion assembly is transferred via the steering column to the steering wheel.

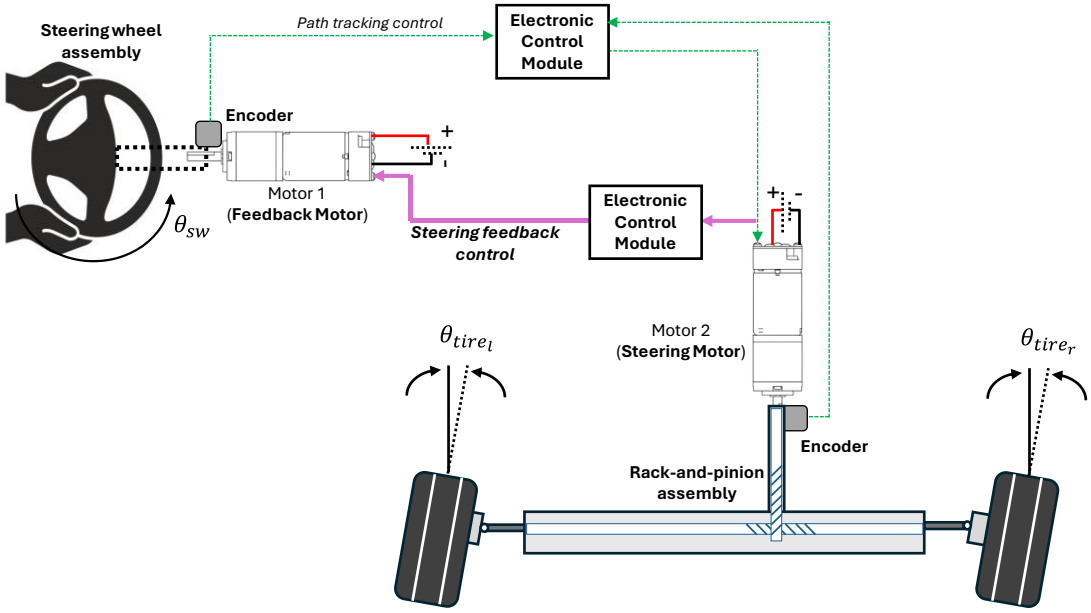

Figure 4. The steering feel design in the SbW architecture

In this study, the development of steering feel in the SbW system was addressed via adaptive torque tracking control, where force and torque were interrelated. To generate the steering feel, if the aim is to control the force value at the motor, it can be regulated through controlling the motor's torque output. The total torque acting on the front wheel assembly is generated by torque motor 2 (refer to Figure 4), driving the front wheels via the rack-and-pinion mechanism. More specifically, the torque produced by motor 2 represented the desired forces, where the forces are from road surface interaction, suspension movements, and tire-road dynamics. By accurately modeling and controlling these forces/torques, the driver can experience the same feel and response at the steering wheel during driving. This approach simplified the development of steering feel (steering feedback) in the SbW system by integrating dynamic elements that varied during vehicle maneuvers. These dynamic elements included changes in yaw rate, lateral acceleration, additional dynamic loads from the front wheel assembly, and frictional forces from system joints. Therefore, to accurately replicate steering feel in the SbW system, the torque transmitted to the steering wheel must mimic the characteristics of torque typically transmitted through a conventional rack-and-pinion assembly. This is crucial for maintaining the desired steering feel and vehicle handling characteristics [71].

To control the torque feedback in real-time, motor 1 in the SbW system continuously adjusted the output torque based on the torque generated by motor 2. This interaction allowed the system to simulate the resistance or disturbance typically felt at the steering wheel by the driver. The torque produced by motor 2 represented the total desired torque, influenced by various factors such as vehicle speed, steering angle, road conditions, and suspension dynamics. Achieving this required precise control algorithms that considered both the vehicle's dynamic state and the driver's steering input. The

system's feedback loop computed the desired torque, T_{m2} based on the forces acting on the front wheel assembly, and adjusted the output of torque motor 1, T_{m1} to match these characteristics. This approach allowed motor 1 to generate torque feedback that closely mirrored the force flow of a traditional rack-and-pinion system, providing the driver with the same level of tactile feedback, confidence, and control. Additionally, this approach is both simple and more accurate for developing steering feel, as the feedback torque at the steering wheel is directly correlated to the torque generated by the rack and pinion assembly, which encompasses all torques from the front wheel components [32],[72]-[75].

Moreover, the torque generated by the motor can be inferred from the current drawn by the motor, as the motor's torque is directly proportional to the current flowing through its windings. When the motor was subjected to a load, the required current increased to overcome the associated resistive forces. This change in current corresponded to a variation in the torque produced. Therefore, by measuring the current supplied to the motor, the resulting torque can be calculated using a known relationship, as specified in equations (25) and (26). This approach allowed real-time torque estimation without the need for direct torque sensors, offering a cost-effective and efficient method for monitoring motor performance [76].

Numerous researchers have developed various controllers to optimize the steering feel in the SbW system. As discussed in section 1.0, controllers from the PID-based category have shown significant effectiveness due to their straightforward feedback mechanism, ease of implementation, and simplicity in tuning and troubleshooting. In this study, a basic control strategy of conventional proportional-integral (PI) control for the SbW system was selected at an early stage, as shown in Figure 5. The control action from the PI controller was triggered by the error signal e(t) obtained from the differences between the actual torque of motor 1, T_{m1}, and the desired torque of motor 2, T_{m2}. Based on the difference between these values, a correction factor was calculated and applied to the input. The general single-input and single-output (SISO) control system with a continuous PI controller action for the SbW plant and the generation of the control signal u(t) can be written in equation (39). The correction factors were calculated by comparing the process variable (output value) to the setpoint and applying the proportional (K_p) and integral (K_i) gains to minimize overshoot, decrease rise time, and reduce settling time, all while affecting the change period as quickly as possible. One of the popular methods for tuning a PI controller is the Zeigler and Nichols method. This approach involves analyzing the system's response to changes, such as measuring the system's oscillation at the ultimate gain (K_u) and the corresponding period of oscillation (P_u). By adjusting the PI parameters based on these observations, the controller can be fine-tuned for optimal performance.

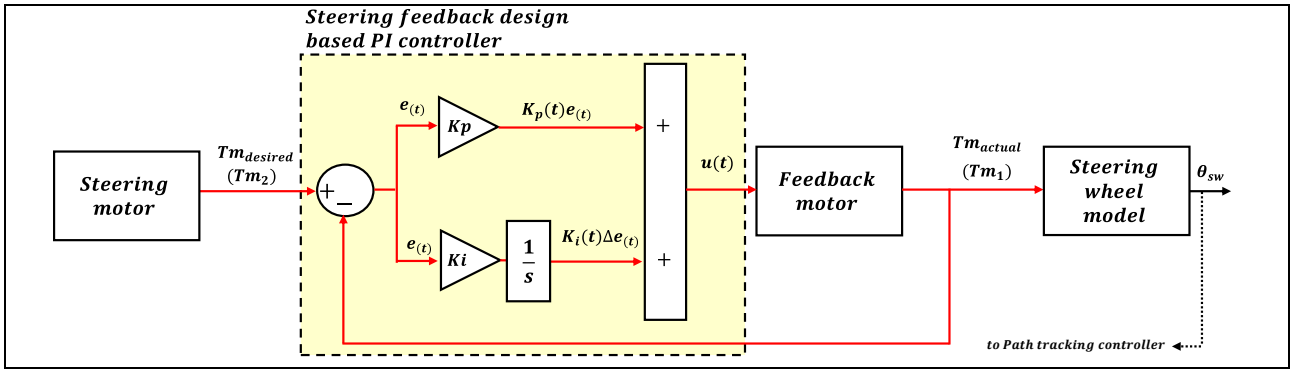

Figure 5. Control strategy PI-based of steering feel design in the SbW model

$$\begin{aligned} u(t) = &\ u(t-1) + \Delta u(t) \\ = &\ u(t-1) + K_i(t)\mathrm{e}(t) + K_p(t)\Delta e(t) \end{aligned} \tag{39}$$

where,

$e(t) =$ $y'(t) + y(t)$ The error between the desired output and the actual output.
$\Delta e(t) =$ $e(t) - e(t-1)$ The change in error (first-order difference).
$u(t-1) =$ The control signal at the previous time step.
$K_p(t) =$ Proportional gain.
$K_i(t) =$ Integral gain.

The primary purpose of a PI controller is to continuously adjust the process output to match the desired setpoint, thereby maintaining stability and accuracy. It is recommended in systems where the load frequently changes, as it allows the controller to compensate automatically for variations in setpoint, energy available, or other variables, ensuring consistent performance even under fluctuating conditions. In addition, this control category is often considered one of the simplest control strategies, yet a powerful mechanistic representation of the universal error feedback law [77]. Its straightforward controller design enables effective control without the need for complex algorithms or significant computational resources, other than the least-cost implementation process [78]. However, this controller may not perform well in dynamic or complex conditions, such as those encountered in real-world applications or case studies. It has been reported that most PI controllers operating in automatic with fixed gains behaved poorly after a certain time than in open-loop operation [79]-[80].

To address this limitation, several researchers have suggested enhancing the traditional PID-based controller's capabilities by evolving it into a dynamic controller, an adaptive controller [81]. Some studies further emphasized the need to upgrade the traditional PID-based controllers to dynamic controllers in order to enhance robustness, particularly in the presence of external disturbances [82]. Additionally, it has been reported that several researchers have implemented metaheuristic algorithms to improve the performance of structured PID-based controllers in numerous application domains, especially in robotics and manufacturing. Therefore, adaptive and gain scheduling methods have emerged as commonly applied methods for non-linear models using PID-based controllers, where the operating conditions of the system are constantly changing [83].

In this section, the concept of steering torque feedback in the SbW system is explored using an adaptive control strategy. The proposed controller operated within a closed-loop feedback framework, integrated with a full vehicle dynamic model and several auxiliary controllers to achieve precise control actions. The key components of the control scheme that were tested included the proportional-integral (PI) controller and adaptive PI-based controllers, both developed using two (2) distinct approaches: an adaptive technique and a gain scheduling technique. Each of these methods is thoroughly discussed in this section. A comprehensive modeling and simulation study is presented to evaluate the performance of the proposed control scheme. The verification process is also outlined, which assesses the controller's ability to maintain effective operation under various input signal conditions. The performance of the adaptive controllers was analyzed in terms of robustness, response time, and accuracy.

3.1 Gain Scheduling Proportional-Integral (GS-PI) Control Strategy

By leveraging the unique characteristics of the PID-based controller, as explained in section 1.0 and section 3.0, the gain scheduling method can enhance the PI controller's performance by adapting its gains in real-time to varying operating conditions. The scheduling mechanism was needed to determine the appropriate PI gains for the current operating point, as the PI controller can only satisfy the design requirements within a specific range of operational conditions. A block diagram of the SbW system with a gain scheduling mechanism for steering feedback control is shown in Figure 6.

Although the concept of associating controller parameters with auxiliary variables is well-established, the practical implementation of gain scheduling remains a significant challenge. In this study, the objective was to optimize the steering torque feedback in the SbW system by utilizing an interpolation and extrapolation-based algorithm for PI gain scheduling and tuning. A set of pre-tuned PI controller gains was determined for a discrete range of vehicle speeds. This control scheme can be used for switching a pre-tuned PI controller to obtain the best performance for each specified vehicle speed. For this reason, the conventional PI gains need to be identified. Simulation work for each vehicle speed must be conducted accordingly. Assuming that the appropriate controller gains for the conventional PI controller have been determined at each vehicle speed, these values can be stored in a parameter table. The appropriate gains were selected based on the scheduling variable corresponding to different ranges of vehicle speed. Using the gain scheduling table, the PI parameter can be reset by interpolation and extrapolation methods according to various vehicle speeds. The controller gains obtained from the simulation results are presented in Table 2.

Table 2. PI controller parameters

Longitudinal speed of vehicle (km/h)	Vehicle Dynamic Test	
	K_p	K_i
20	0.69	-0.05
40	1.80	-0.35
60	3.50	-0.89
80	5.50	-1.90
100	5.75	-4.40
120	7.00	-5.00

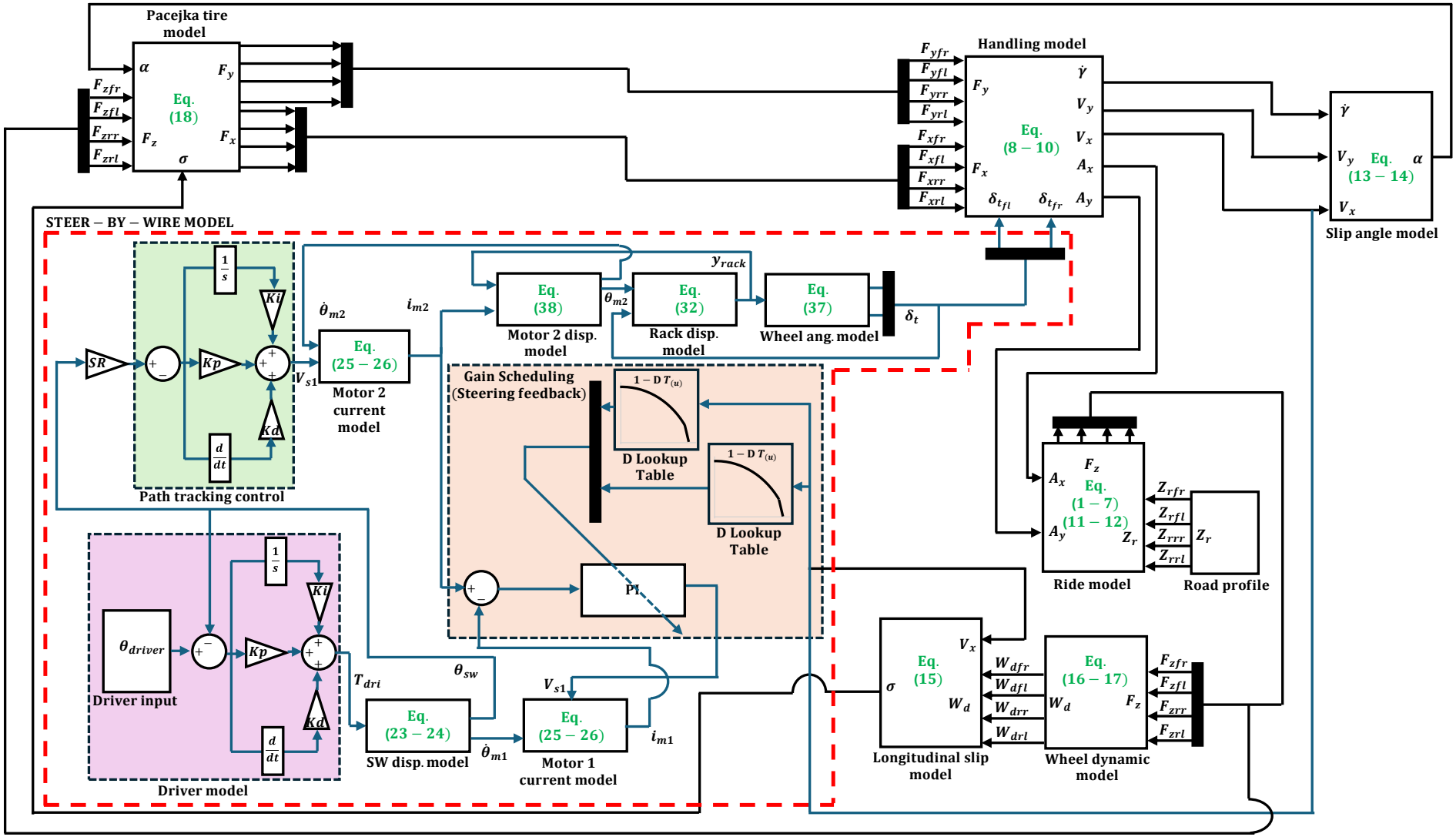

Figure 6. Gain Scheduling PI (GS-PI) controller in SbW-14DOF model

3.2 Adaptive Proportional-Integral (A-PI) Control Strategy

Based on previous research, one of the nonlinear controllers explored is the adaptive PI (A-PI) controller. A-PI controller adjusts its parameters, specifically the proportional and integral gains, in real time in response to changes in system behavior or environmental conditions. This controller can maintain optimal performance in the presence of dynamics such as non-linearity, parameter variations, or external disturbances. The A-PI controller can continuously modify its tuning parameters to respond to these variations, making it more versatile and effective in managing a broader range of dynamic processes. Figure 8 illustrates the implementation of the A-PI controller within the SbW model represented in MATLAB Simulink block diagram.

To design the linearization equation for the adaptive gains, it is first necessary to characterize the conventional PI controller's gains across a range of input conditions using a simulation model. This step is crucial for identifying any potential issues in the PI controller's performance during transitions between low and high vehicle speeds. Such analysis is particularly important to ensure that the controller operates effectively under varying speed conditions.

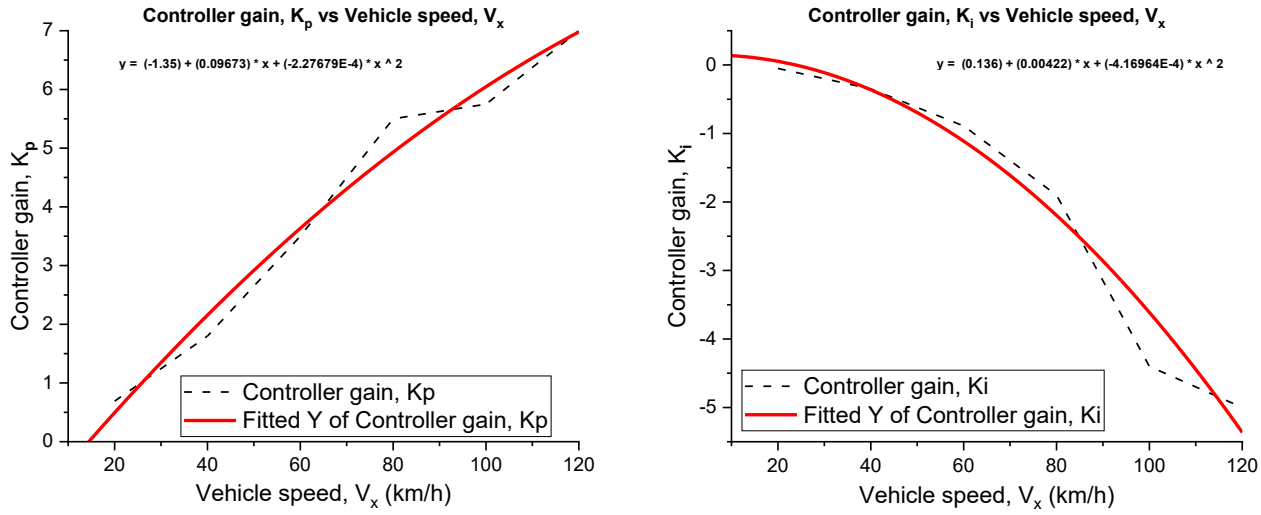

(a) (b)

Figure 7. Controller gain versus vehicle speed, (a) K_p gain and (b) K_i gain.

Based on the results obtained from the simulation test (refer Table 2), the A-PI controller was designed with both K_p and K_i gains expressed as dynamic mathematical equations. The corresponding plots for K_p and K_i are shown in Figure 7. These expressions allow the K_p and K_i gains to function as dynamic factors, thereby transforming the linear PI controller into a nonlinear PI controller. The mathematical formulations for both gains in the adaptive control system are presented in equations (40) and (41).

$$K_p = -0.0002277\ (v_x)^2 + 0.09673\ (v_x) - 1.35 \tag{40}$$

$$K_i = -0.000417\ (v_x)^2 + 0.004218\ (v_x) + 0.136 \tag{41}$$

where v_x is the longitudinal speed of the vehicle.

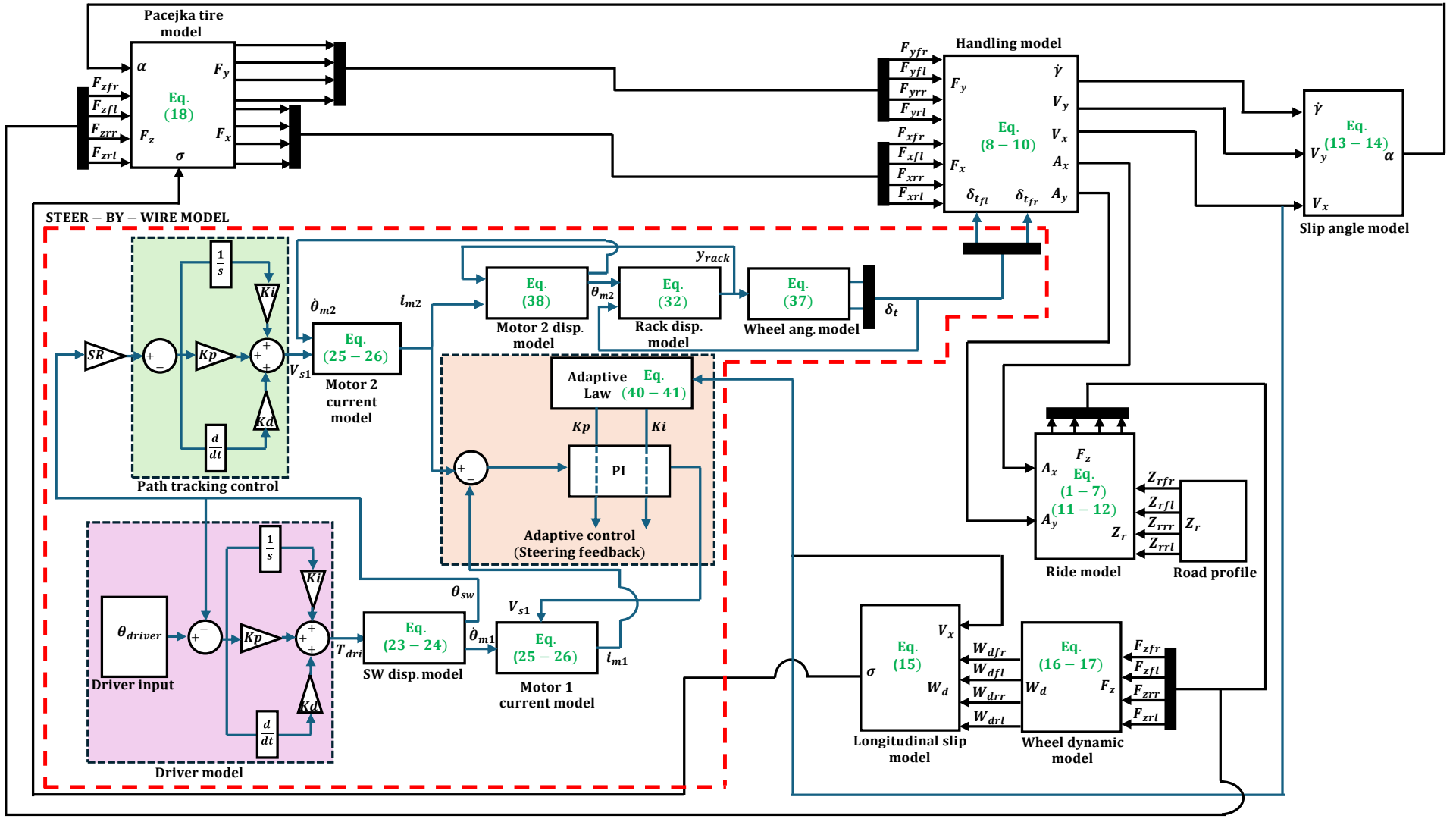

Figure 8. Adaptive PI (A-PI) controller in SbW-14DOF model

3.3 Verification of Proposed Control Strategy

To assess the performance of the GS-PI and A-PI controllers in the SbW system, a verification process was performed using a set of test input signals. Based on Figure 9, two (2) different types of signal inputs were applied to the SbW model through MATLAB Simulink: a step input wave and a sinusoidal wave. These signal types were selected to evaluate the controller's response in terms of response time, stability, and transient behavior under various dynamic conditions that could occur in real-world applications. The step input signal was used to evaluate how effectively the control system deals with sudden changes in input, such as abrupt steering action by the driver. In contrast, the sinusoidal wave input assessed the control system's performance under steady-state oscillations, determining whether it can maintain a consistent output over time without introducing undesirable phase lag or amplitude distortion.

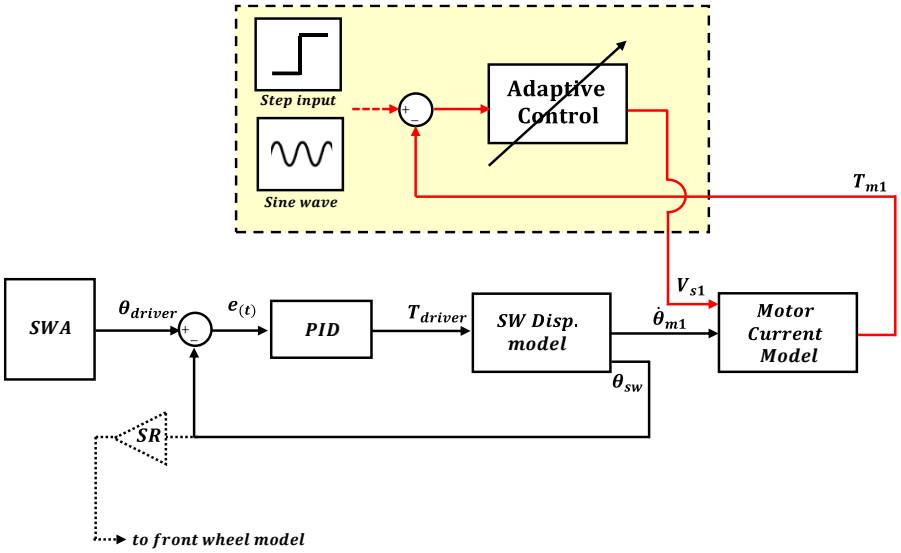

Figure 9. Controller gain versus vehicle speed, (a) K_p gain and (b) K_i gain

At the verification stage, the investigation focused only on the steering wheel model to assess the performance of the steering torque feedback system, using both step and sinusoidal input signals. These signals served as reference inputs, representing the torque generated by motor 2. The primary goal of this stage was to determine whether both adaptive controllers could effectively track the reference signal. The longitudinal vehicle speed was defined within a range, with minimum and maximum values of 40 km/h and 100 km/h, respectively. This speed range was selected to evaluate the control system's performance under both low and high speed conditions. At low speeds, the steering torque requirement is minimal, while at high speeds, the steering torque demand is higher. This selection aligns with findings from studies, such as those by He et al. [84], Choi et al. [85], and Zhang et al. [86], which suggested that testing at the extreme of the speed range provides adequate verification for typical driving scenarios.

In this context, the steering wheel torque was set to 1.5 Nm for low-speed conditions and 5.0 Nm for high-speed conditions. This torque range was selected based on existing literature and previous research work, which indicates that typical passenger vehicles require steering torques ranging from approximately 1.0 Nm to 8.0 Nm for the motor (actuator) in an SbW system [25],[87]-[89]. To facilitate the verification process, the step input and sinusoidal input signals were applied with amplitudes of 1.5 Nm and 5.0 Nm, respectively, corresponding to low and high speed vehicle conditions. These key parameters were established to ensure accurate simulation of the SbW system's performance. The resulting simulation outcomes for each input signal are presented in Figure 10 and Figure 11.

As illustrated in Figure 10(a) and Figure 10(b), both the A-PI and GS-PI controllers exhibited stable responses to the step input signal at vehicle speeds of 40 km/h and 100 km/h. No overshoot or oscillatory behavior was observed, demonstrating the controllers' robustness in handling sudden torque demand changes. The detailed transient response parameters, including rise time and settling time, are summarized in Table 3.

Table 3. Settling and rise time for each vehicle speed (step input signal)

Controller	v_x = 40 km/h		v_x = 100 km/h	
	Settling time (sec)	Rise time (sec)	Settling time (sec)	Rise time (sec)
Gain Scheduling PI (GS-PI)	3.0100	3.0031	3.0170	3.0025
Adaptive PI (A-PI)	3.0230	3.0035	3.0340	3.0029

The GS-PI controller consistently achieved slightly faster rise and settling times compared to the A-PI controller, particularly evident at higher vehicle speeds. This improvement indicates the effectiveness of the gain-scheduling

mechanism in adapting to variations in dynamic conditions. Both controllers accurately tracked the reference torque magnitude,T_{m2}, as shown by the minimal steady-state error. The enlarged view of the transient region highlights the smoother response of the GS-PI controller, which reached the target torque more rapidly and with reduced lag relative to the A-PI controller. These findings suggest that while both controllers can reliably reproduce the desired torque profile under abrupt input changes, the GS-PI design offers enhanced adaptability across a wider range of operating conditions.

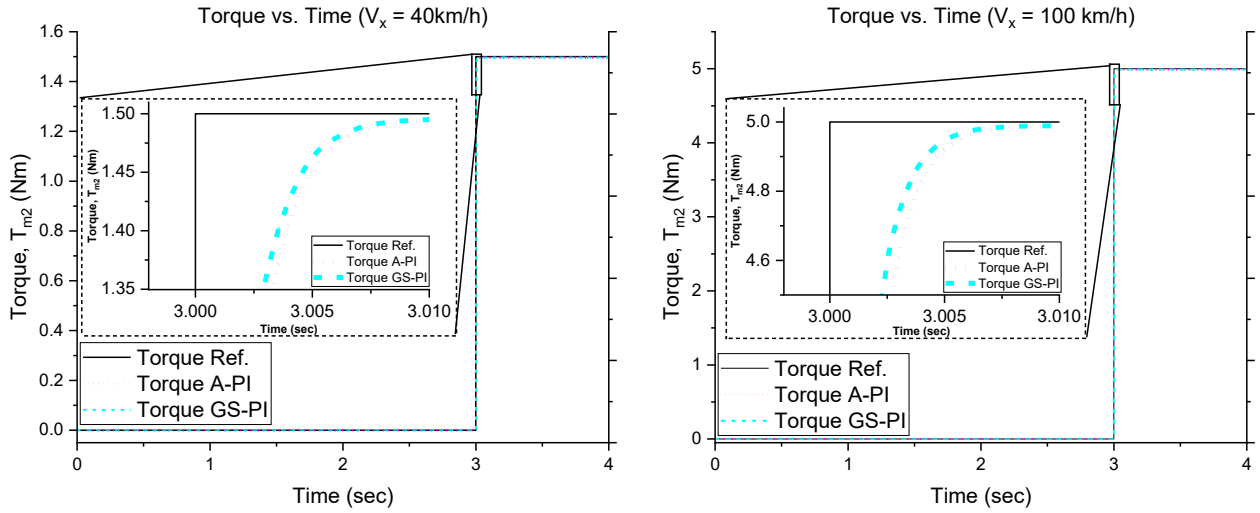

(a) (b)

Figure 10. The performance of the A-PI and GS-PI controllers under different speeds of the vehicle for a step input signal: (a) 40 km/h and (b) 100 km/h

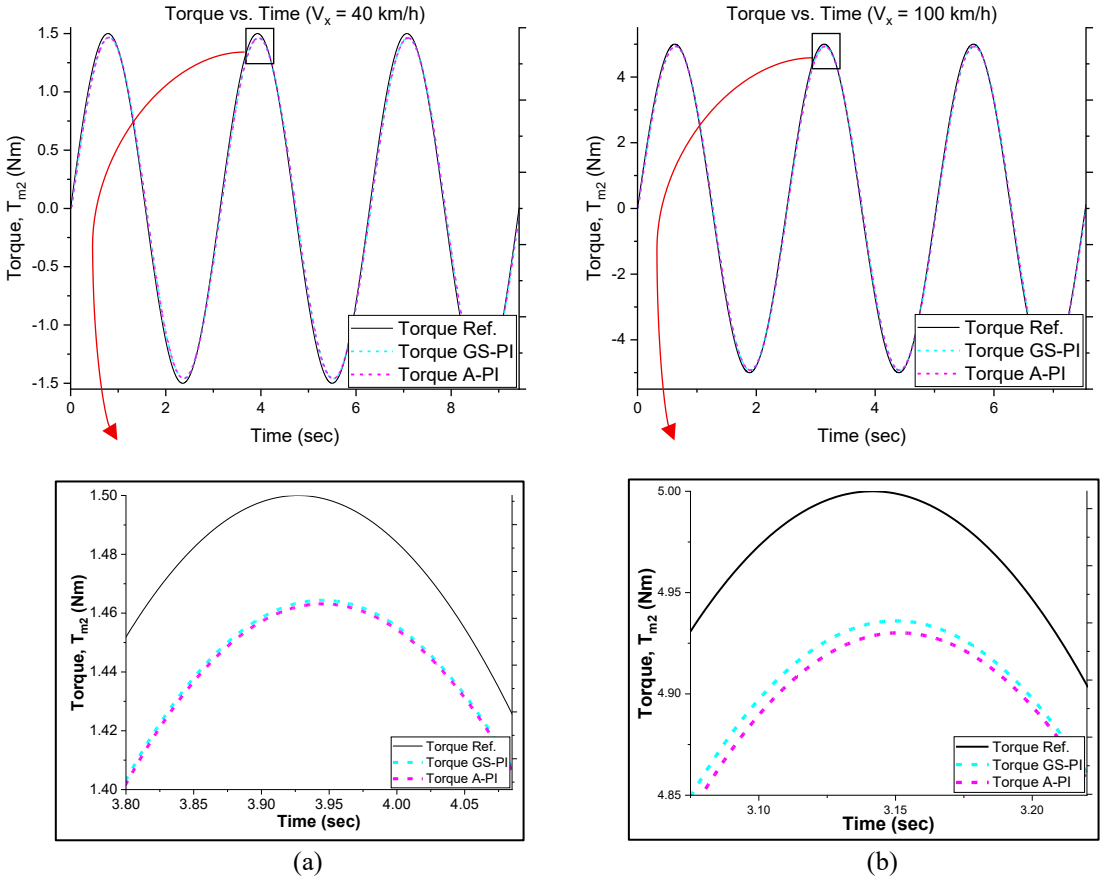

(a) (b)

Figure 11. The performance of the A-PI and GS-PI controllers under different speeds of the vehicle for a sinusoidal input signal: (a) 40 km/h and (b) 100 km/h

Figure 11(a) and Figure 11(b) illustrate the response of both controllers to a sinusoidal torque input at vehicle speeds of 40 km/h and 100 km/h. The A-PI and GS-PI controllers successfully maintained stable tracking across the entire input cycle, with no irregular oscillations or distortion observed. Minor deviations in tracking performance were noted, primarily in the form of phase lag and slight amplitude attenuation relative to the reference signal. The GS-PI controller

consistently reduced these deviations compared to the A-PI controller, particularly at high vehicle speed conditions. This improvement highlights the benefit of gain scheduling in adapting control effort to changing dynamic loads. Overall, the ability of both controllers to maintain the desired torque waveform with minimal tracking error under continuous input variations reinforces their robustness. Section 4.0 discusses the performance of both controllers to track torque through validation against the ISO-standard vehicle dynamic test.

4. RESULTS AND DISCUSSION

The verification results demonstrated the ability of both adaptive controllers to accurately track the input signals, with the simulation results indicating high precision, as discussed in subsection 3.3. This confirmed that both controllers were capable of effectively tracking any applied input signals. To further evaluate the performance of both controllers, this section presents validation results when subjected to real-world vehicle dynamic tests. A simulation study was conducted to examine the capability and potential benefits of the proposed controller in developing steering feedback at the steering wheel. The test employed in this study followed standard vehicle dynamics protocols as defined by ISO standards. Specifically, the study utilized the Double Lane Change (DLC) Test (ISO 3888), Slalom (SL) test (ISO 13674-2), and J-Turn (JT) test (ISO 7401). The speed profiles and steering angles used in these tests are presented in Table 4.

Table 4. Speed profiles and steering angle for each test

Vehicle dynamic test	Parameter Profiles		Aim
	Speed (km/h)	Steering Wheel Angle (deg.)	
DLC	100	-	High speed scenario
SL	50	-	Middle speed scenario
JT	20	330	Low speed scenario

The primary objective of the dynamic tests is to evaluate the adaptability of the proposed controller under varying vehicle dynamics conditions. The DLC test is specifically designed to assess the handling characteristics of a vehicle during rapid directional changes at high vehicle speeds, making it ideal for understanding the controller's performance in high-speed scenarios. Additionally, this dynamic test facilitates the assessment of steering wheel sensitivity and precision, particularly in situations where the driver must respond quickly to avoid obstacles. In this study, the vehicle accelerated from the starting line to 100 km/h and maintained this speed throughout the course to complete the DLC test. The SL test, on the other hand, focuses on the vehicle's responsiveness and precision during a repeated series of rapid steering maneuvers, providing valuable insight into the ability of the controller to manage transient steering events effectively. This test involves a predefined course marked by a series of cones arranged in a zig-zag pattern, with cone spacing ranging from 7 to 10 metres. The driver or vehicle must navigate through this course at varying speeds. During this test, the vehicle maintained a constant speed of 50 km/h from the starting point to the endpoint during the SL test.

Finally, the JT test is designed to evaluate the vehicle's handling characteristics during low-speed maneuvers, such as tight cornering, allowing for an assessment of the controller's performance under constrained steering conditions. In this test, the vehicle initially traveled in a straight line at 20 km/h before executing the first steering input, involving a 330° turn in one direction within 2.25 seconds. The first steering angle was determined by multiplying the steering wheel angle that produced a steady-state lateral acceleration of 0.3 g at 20 km/h on pavement by a factor of 8, and this angle was held for 4 seconds. This was followed by a counter-steer, where the steering wheel returned to its initial position, from 330° to 0°, within 2 seconds.

In this study, the results obtained from CarSim, a certified vehicle dynamic simulation software, were used as the benchmark for each vehicle dynamic test. The vehicle model parameters used in MATLAB Simulink are provided in Appendix C. For the validation stage, the 2017 Hatchback model, selected from the A-class vehicle chassis type parameter, was employed. The performance of both adaptive controllers was evaluated not only by analyzing the changes in steering wheel torque over time but also by examining the changes in rack displacement at the rack and pinion assembly, the steering wheel angle, and wheel steer angle. Although an auxiliary PID controller was employed for path tracking of the wheel steer angle, its design and implementation have been discussed in [60]. Nevertheless, it is essential to monitor the system to ensure that the adaptive controller responsible for torque tracking does not introduce unintended disturbances or adversely affect the path tracking controller's performance.

From the DLC test results at 100 km/h, the steering torque feedback controller's performance, as shown in Figure 12(a), reveals that the steering wheel torque produced by the GS-PI controller more closely matched the CarSim software results in both magnitude and trend, compared to the PI and A-PI controllers. This suggested that the GS-PI controller more accurately replicated the expected steering torque response, providing improved feedback. However, some initial overshoot and fluctuation were observed from all controllers, which could indicate sensitivity during the transition into the maneuver. Additionally, the closer match between the GS-PI controller and the CarSim model can be attributed to its more effective adaptation to changing vehicle dynamics.

As depicted in Figure 12(b) and Figure 12(c), the GS-PI controller demonstrated better consistency and fidelity across varying lateral acceleration values. In contrast, the PI and A-PI controllers tended to overshoot the expected steering wheel torque magnitude when compared to the CarSim model. This overshoot could lead to overcompensation in steering forces, potentially disrupting the natural feel of the steering feedback and making the steering wheel less responsive and less intuitive for the driver. At a higher positive or negative lateral acceleration value, a_y, the A-PI controller's response failed to match the steering wheel torque magnitude produced by the CarSim model, the same as the PI controller. In other words, under extreme cornering conditions, where high a_y values are encountered, the mismatch between the PI and A-PI controller and the CarSim reference could result in nonlinear behavior that may affect the steering feel. A comparison of the mean absolute error (MAE) in steering wheel torque further supported this observation, with the GS-PI controller achieving a lower MAE of 1.826, compared to 2.109 and 2.106 for the PI and A-PI controllers.

Furthermore, all controllers exhibited a similar pattern with only slight variations in magnitude for both steering wheel angle performance and wheel steer angle performance, as illustrated in Figure 13(a) to Figure 13(b). The graph indicated no significant changes in either magnitude or trend across the controllers. In other words, the torque tracking controller does not have a significant impact on changes in steering wheel angle and wheel steer angle. The MAE in rack displacement at the rack and pinion assembly was relatively minor, with the GS-PI controller exhibiting an error of 1.016, while the PI and A-PI controllers exhibited errors of 1.022 and 1.021, respectively. The movement closely followed the expected trends, with only slight variations in magnitude, as illustrated in Figure 13(c).

For the SL test conducted at 50 km/h vehicle speed, the GS-PI controller demonstrated better tracking of steering wheel torque, as shown in Figure 14(a). Both the GS-PI and A-PI controllers exhibited the ability to track the steering wheel torque. However, the GS-PI controller maintained better alignment with the overall trend, with only slight variations in magnitude. In contrast, while the A-PI controller was able to track the general trend of the steering wheel torque compared to the CarSim results, it demonstrated noticeable lag during rapid torque transitions, which affected the magnitude of the steering wheel torque over time. These findings indicated that the GS-PI controller imparted more effective torque tracking performance in this vehicle dynamic test compared to the A-PI controller. The MAE value for the GS-PI controller was 1.997, whereas the A-PI controller produced a higher MAE error of approximately 2.125. In comparison, the PI controller exhibited a significantly higher MAE value of over 10, indicating its inability to effectively track the steering torque in the SbW system.

As illustrated in Figure 14(b) and Figure 14(c), the GS-PI controller provided better alignment with the benchmark, CarSim results, both in terms of magnitude and overall trend. This indicated that the GS-PI controller delivered a more realistic steering feedback experience for the driver. Conversely, the A-PI controller showed reduced precision in replicating the intricate variations in steering torque at higher lateral acceleration,a_y and exhibited limited adaptability to rapid changes in lateral forces. It also showed an overshoot phenomenon during maneuvers, leading to unpleasant steering behavior that may compromise the driver's steering feel. Additionally, the A-PI controller operated within a narrower and less linear torque range, indicating suboptimal response under high steering wheel demands.

Moreover, it was observed that neither adaptive controller significantly affected the steering wheel angle and wheel steer angle over time. As shown in Figure 15(a) and Figure 15(b), both adaptive controllers exhibit that the magnitude and overall trend of steering wheel angle and wheel steer angle closely follow the benchmark, CarSim model, with only minor variations in magnitude. Additionally, Figure 15(c) illustrates that the pattern and trend of rack displacement at the rack and pinion assembly remain consistent, with MAE values of 0.443 for the GS-PI controller, 0.446 for the A-PI controller, and 0.625 for the PI controller. Both controllers' magnitude and trend aligned closely with the CarSim results. However, the PI controller exhibited abnormal behavior, causing noticeable deviations in both the steering wheel angle and wheel steer angle.

For the JT test at 330° and 20 km/h vehicle speed, as illustrated in Figure 16(a), the GS-PI controller exhibited better tracking accuracy compared to the A-PI controller. The GS-PI controller closely replicated the steering wheel torque of the benchmark, CarSim model, indicating its greater capability to accurately reflect steering feedback characteristics at the steering wheel. The MAE value for the GS-PI controller was about 2.477, significantly lower than that of the A-PI controller, 5.326. Based on Figure 16(b) and Figure 16(c), the GS-PI controller also exhibited better tracking performance, particularly when responding to steering wheel angle demands in the linear region. In contrast, the A-PI controller was less accurate and demonstrated a noticeable offset from the benchmark. During high lateral acceleration, the A-PI controller exhibited torque overshoot after the vehicle entered the second maneuver around the 6-second mark, suggesting the A-PI controller was overly sensitive during the transition between maneuvers. Meanwhile, the PI controller failed to track the steering torque in the SbW system, with a MAE value exceeding 10.

Additionally, as shown in Figure 17(a) and Figure 17(b), all controllers demonstrated that there was no negative impact on the changes in steering wheel angle and wheel steer angle. This indicated that none of the controllers interfered with the path tracking controller's ability to follow the desired steering wheel angle and convert it into the appropriate wheel steer angle. The rack displacement in the rack and pinion assembly also closely followed the benchmark pattern, from the CarSim model, exhibiting an MAE value of 0.030 for the GS-PI controller, 0.032 for the A-PI controller, and 0.077 for the PI controller with only minor variations in magnitude, as illustrated in Figure 17(c).

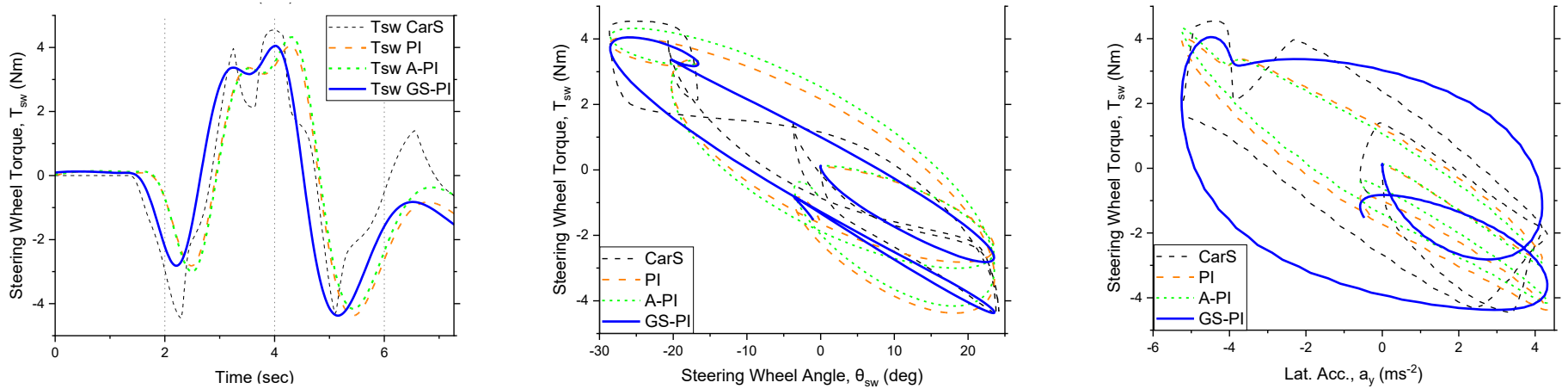

Figure 12. The performance of the PI, A-PI, and GS-PI controllers under DLC test scenarios: (a) steering wheel torque vs. time, (b) steering wheel torque vs. steering wheel angle, and (c) steering wheel torque vs. lateral acceleration

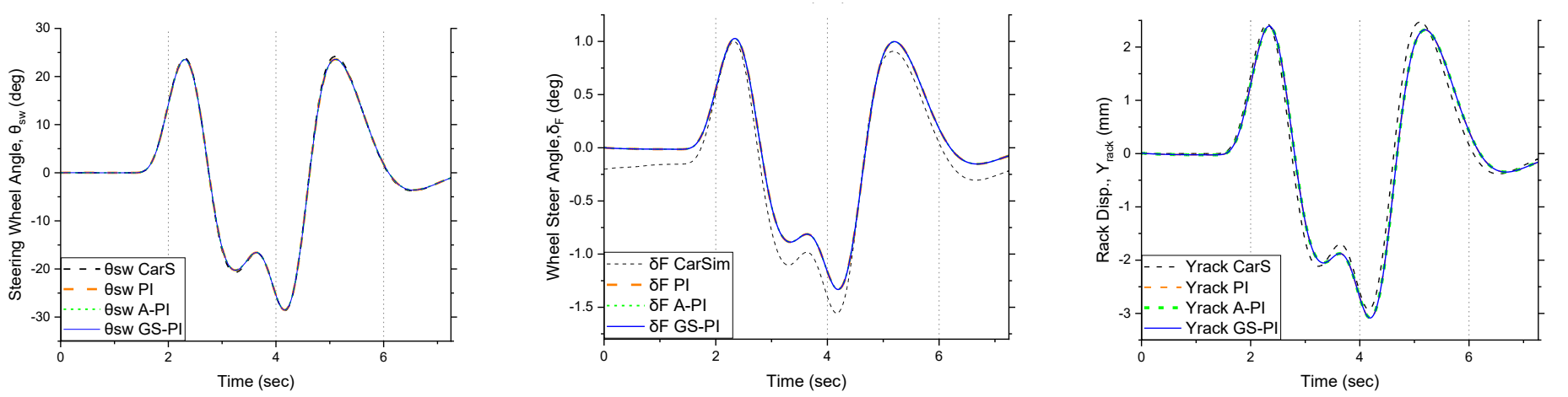

Figure 13. The performance of the PI, A-PI, and GS-PI controllers under DLC test scenarios: (a) steering wheel angle vs. time, (b) wheel steer angle vs. time, and (c) rack displacement vs. time

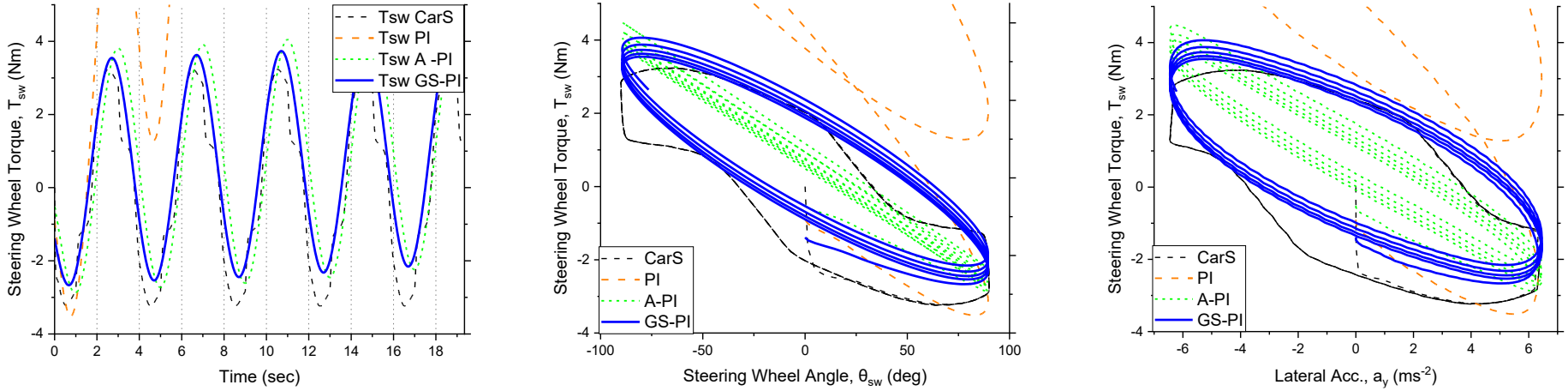

(a) (b) (c)

Figure 14. The performance of the PI, A-PI, and GS-PI controllers under SL test scenarios: (a) steering wheel torque vs. time, (b) steering wheel torque vs. steering wheel angle, and (c) steering wheel torque vs. lateral acceleration

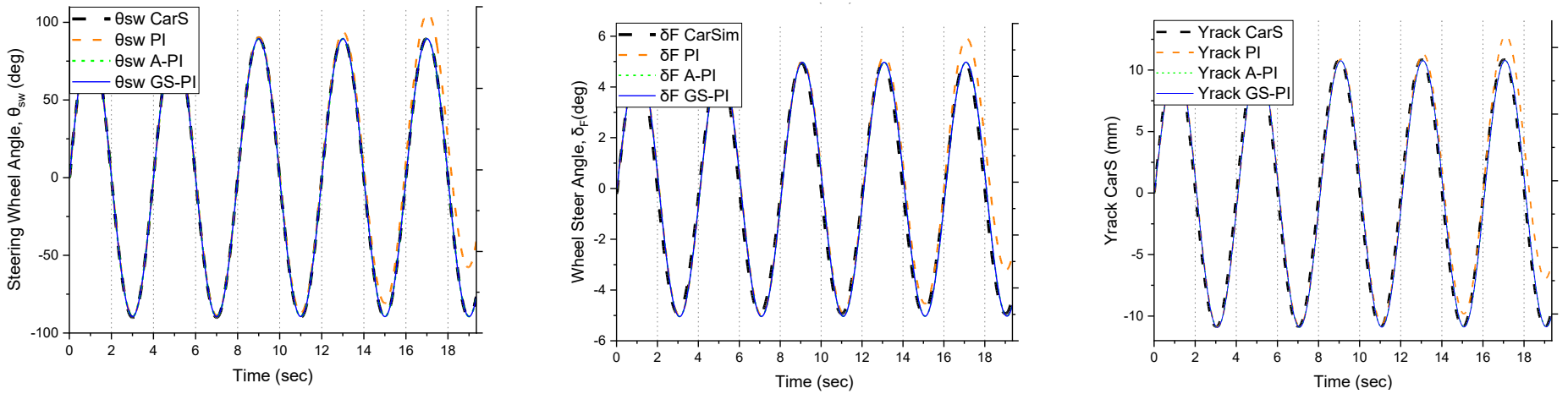

(a) (b) (c)

Figure 15. The performance of the PI, A-PI, and GS-PI controllers under SL test scenarios: (a) steering wheel angle vs. time, (b) wheel steer angle vs. time, and (c) rack displacement vs. time

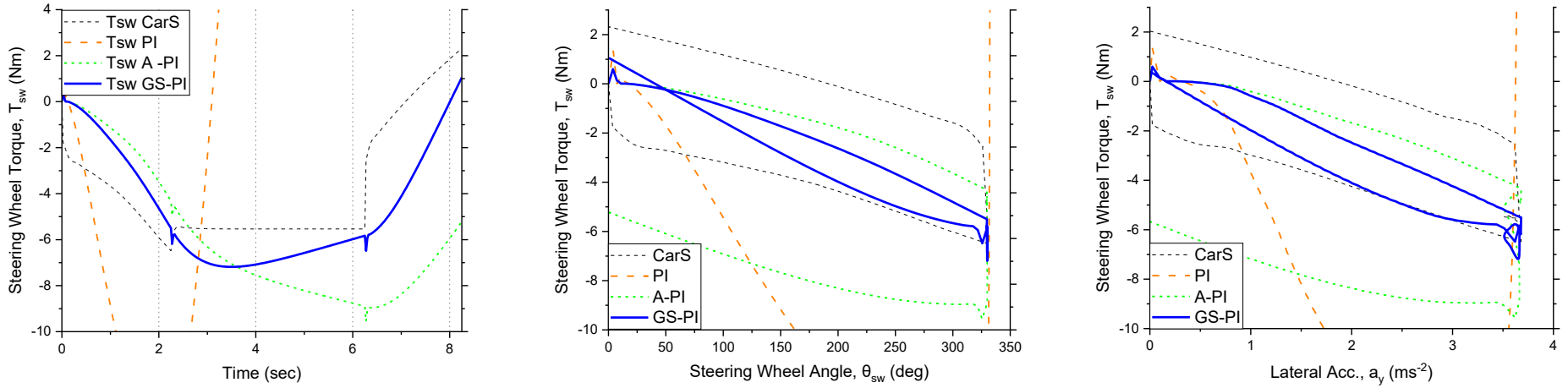

(a) (b) (c)

Figure 16. The performance of the PI, A-PI, and GS-PI controllers under JT test scenarios: (a) steering wheel torque vs. time, (b) steering wheel torque vs. steering wheel angle, and (c) steering wheel torque vs. lateral acceleration

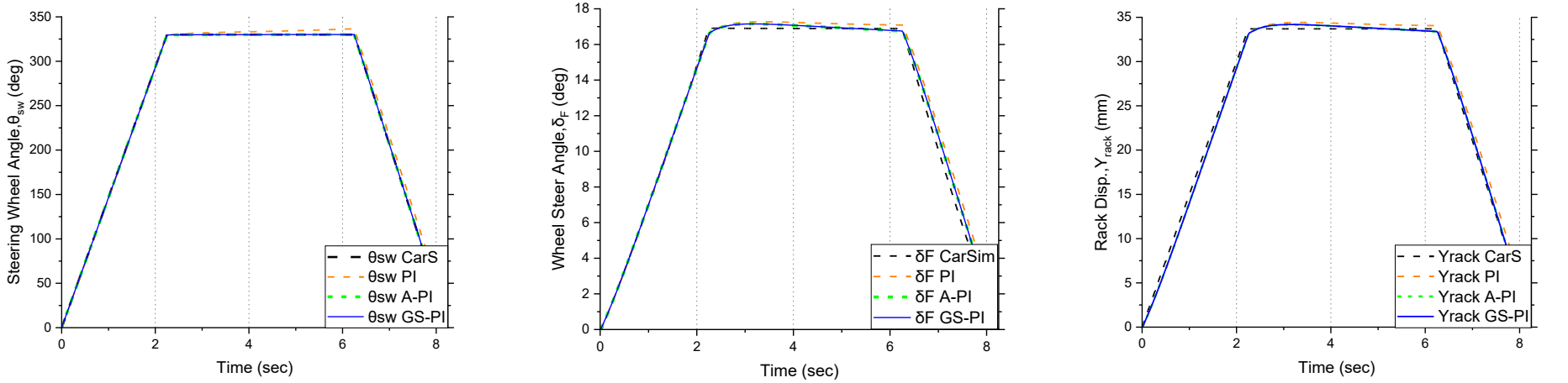

(a) (b) (c)

Figure 17. The performance of the PI, A-PI, and GS-PI controllers under JT test scenarios: (a) steering wheel angle vs. time, (b) wheel steer angle vs. time, and (c) rack displacement vs. time

Table 5 presents the MAE values for each controller under various vehicle dynamic test conditions. The GS-PI controller demonstrated superior torque tracking performance in the DLC, SL, and JT tests. With MAE values ranging approximately from 1.8 to 2.5, the GS-PI controller exhibited a high level of accuracy in torque control. These findings highlighted the potential for the GS-PI controller in steering feel development within the SbW system, supporting its effectiveness in steering feedback enhancement. Additionally, the results suggested that the PI controller was only effective under specific conditions. While it successfully tracked steering torque during the DLC test, it exhibited poor performance during the SL and JT tests, indicating its limited applicability in more dynamic scenarios.

Table 5. Mean absolute error (MAE) for each test

Controller	Mean Absolute Error (MAE)					
	DLC		SL		JT	
	SWT	Rack Disp.	SWT	Rack Disp.	SWT	Rack Disp.
GS-PI	1.826	1.016	1.997	0.443	2.477	0.030
A-PI	2.106	1.021	2.125	0.446	5.326	0.032
PI	2.109	1.022	>10	0.625	>10	0.077

Future research will focus on the implementation of the GS-PI controller within the SbW system to further assess its impact and benefits. This study is currently in progress, with the SbW system already installed in the test vehicle. Hardware integration involving the motor, microcontroller, and encoders is underway for the upcoming experimental work. Figure 18 illustrates the fully integrated SbW system in the vehicle, with the installed motor, encoder, and microcontroller.

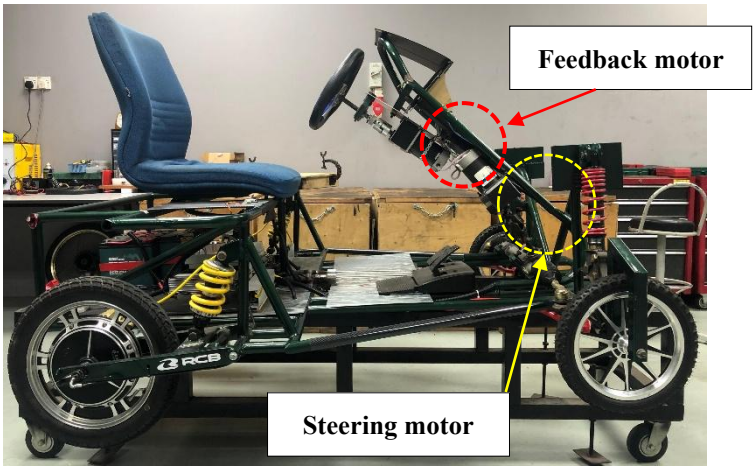

(a)

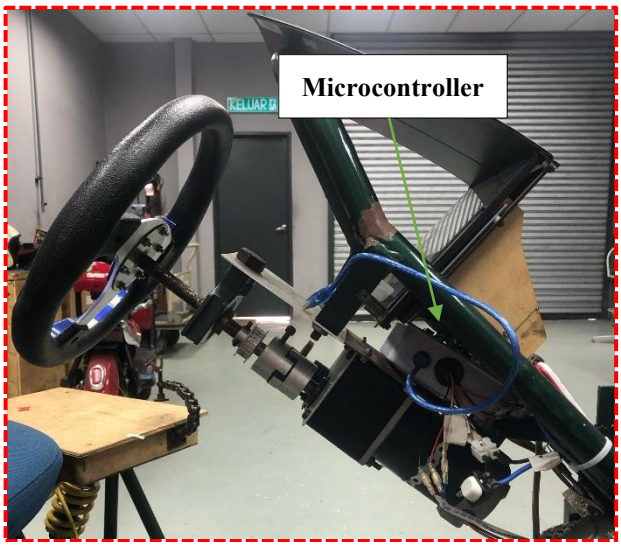

(b)

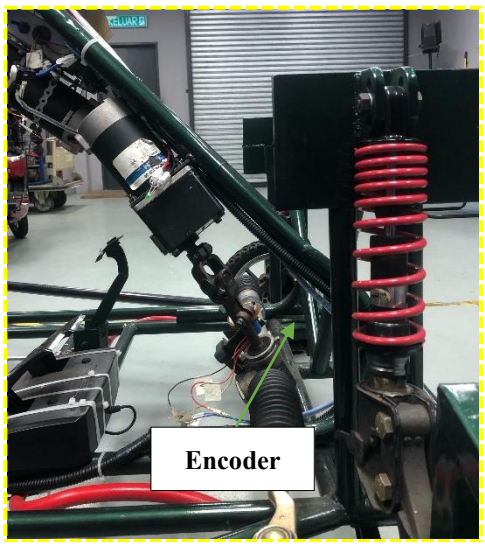

(c)

Figure 18. The SbW system in EV vehicle: (a) steering wheel angle vs. time, (b) feedback motor (Motor 1), and (c) steering motor (Motor 2)

5. CONCLUSIONS

This study addressed the challenge of replicating realistic steering feel in steer-by-wire (SbW) systems through the development of two adaptive PI-based controllers, implemented within a high-fidelity 14-degree-of-freedom (14-DOF) vehicle dynamic model. Two distinct adaptation strategies were proposed: a gain scheduling method and an adaptive tuning method, both designed to allow proportional and integral gains to vary in response to dynamic driving conditions. Simulation results demonstrated that the gain scheduling PI-based (GS-PI) controller provided superior performance in reproducing the desired steering feel, closely approximating the behavior of conventional steering systems modeled in CarSim. Across multiple ISO-standard tests including the Double Lane Change (DLC) at 100 km/h, Slalom (SL) at 50 km/h, and J-Turn (JT) at 20 km/h with 330° steering input the GS-PI controller consistently achieved a mean absolute error (MAE) of less than 2.5, confirming its ability to handle nonlinear vehicle responses under varying conditions. These findings contribute to the field by offering a practical and computationally efficient control solution, bridging the gap between simulation-based studies and real-world hardware implementation.

While much of the existing literature on advanced control strategies remains at the proof-of-concept stage, the methods presented in this study demonstrate strong potential for real-time deployment, particularly in embedded systems with limited processing capabilities. Future work should prioritize the integration of steering torque feedback into hardware platforms, supported by rigorous validation through Hardware-in-the-Loop (HiL) systems and experimental testing under real driving conditions. Additionally, incorporating human-in-the-loop evaluations will be essential to assess the subjective quality of steering feel and driver acceptance. Such efforts will enable a more comprehensive understanding of the proposed controllers' effectiveness, supporting their application in commercial SbW systems and advancing the development of driver-centric vehicle control technologies.

ACKNOWLEDGEMENTS

This study is funded by Universiti Teknikal Malaysia Melaka (UTeM) through the Short Term Grant Research, No: PJP/2024/FTKM/PERINTIS/SA0027. The authors would like to express the gratitude to Universiti Teknikal Malaysia Melaka (UTeM) for providing feasible research facilities for this research work. Additionally, the first author wishes to thank the Malaysian Ministry of Higher Education (MOHE) and Universiti Tun Hussein Onn Malaysia (UTHM) for providing the fellowship program that supported the PhD studies.

CONFLICT OF INTEREST

All authors have agreed with the contents of the manuscripts, and there are no financial or non-financial interests to report.

AUTHORS CONTRIBUTION

M. A. Azizul (Methodology; Data Curation; Writing- original draft; Writing – editing)

F. Ahmad (Conceptualization; Visualisation; Model Verification; Supervision)

J. Karjanto (Funding acquisition; Writing – review; Visualisation; Supervision)

M. H. Md Isa (Visualisation; Funding acquisition)

N. Mohamed (Visualisation; Data Interpretation)

REFERENCES

[1] J. F. Arango, L. M. Bergasa, P. A. Revenga, *et al.*, "Drive-by-wire development process based on ros for an autonomous electric vehicle," *Sensors*, vol. 20, no. 21, pp. 6121, 2020.

[2] A. Kırlı, Y. Chen, C. E. Okwudire, and A. G. Ulsoy, "Torque-vectoring-based backup steering strategy for steer-by-wire autonomous vehicles with vehicle stability control," *IEEE Transactions on Vehicular Technology*, vol. 68, no. 8, pp. 7319-7328, 2019.

[3] M. Li and L. Eckstein, "Fail-operational steer-by-wire system for autonomous vehicles," in *2019 IEEE International Conference on Vehicular Electronics and Safety (ICVES)*, Cairo, Egypt, 2019, pp. 1-6.

[4] K. Chen, X. Pei, D. Sun, Z. Chen, X. Guo, and K. Guo, "Active steering control for autonomous vehicles based on a driver-in-the-loop platform: A case study of collision avoidance," *Proceedings of the Institution of Mechanical Engineers, Part I: Journal of Systems and Control Engineering*, vol. 233, no. 10, pp. 1422–1437, 2019.

[5] S. A. Mortazavizadeh, A. Ghaderi, M. Ebrahimi, and M. Hajian, "Recent developments in the vehicle steer-by-wire system," *IEEE Transactions on Transportation Electrification*, vol. 6, no. 3, pp. 1226-1235, 2020.

[6] G. Perozzi, J.J. Rath, C. Sentouh, J. Floris, and J.C. Popieul, "Lateral shared sliding mode control for lane keeping assist system in steer-by-wire vehicles: Theory and experiments," *IEEE Transactions Intelligent Vehicles*, vol. 8, no. 4, pp. 3073–3082, 2023.

[7] H. Muslim, "Design and evaluation of lane-change collision avoidance systems in semi-automated driving," *IEEE Transactions on Vehicular Technology*, vol. 72, no. 6, pp. 7082–7094, Jun. 2023.

[8] M. H. Hamdi, F. Ahmad, M. H. Che Hasan, M. H. Harun, and V. Rau Aparow, "Model reference adaptive control of an independent steer-by-wire system: A simulation using a 14-degree-of-freedom vehicle model," *International Journal of Automotive and Mechanical Engineering*, vol. 21, no. 4, pp. 11723–11743, 2024.

[9] H. Zhao, B. Wang, G. Zhang, and Y. Feng, "Energy saving design and control of steering wheel system of steering by wire vehicle," *IEEE Access*, vol. 7, pp. 44307-44316, 2019.

[10] J. H. Choi, K. Nam, and S. Oh, "Steering feel improvement by mathematical modeling of the electric power steering system," *Mechatronics*, vol. 78, no. 102629, 2021.

[11] S. H. Kim and C. N. Chu, "A new manual Steering torque estimation model for steer-by-wire systems," *Proceedings of the Institution of Mechanical Engineers, Part D: Journal of Automobile Engineering,* vol. 230, issue 7, pp. 993-1008. 2016.

[12] C. Wang, L. Yan, X. Wu, and Z. Kong, "Design of reconfigurable steering feel for steer-by-wire system based on dynamic load observation," in *2023 7th CAA International Conference on Vehicular Control and Intelligence (CVCI)*, Changsha, China, 2023, pp. 1-7.

[13] I. Chung, S. Oh, and K. Nam, "Synchronous control of a dual-motor driving rack and pinion module for steer-by-wire system," *IEEE Access*, vol. 12, pp. 195358-195369, 2024.

[14] C. Su, H. Li, B. Qiao, *et al.*, "Personalized steering feel design for steer-by-wire systems based on the rack force estimation," *International Journal of Automotive Technology,* vol. 24, pp. 1151–1161, 2023.

[15] T. Chugh, F. Bruzelius, M. Klomp, and B. Jacobson, "Steering feedback transparency using rack force observer," *IEEE/ASME Transactions on Mechatronics*, vol. 27, no. 5, pp. 3853-3864, 2022.

[16] L. Zhao, X. Zhao, and H. Li, "Rack force fault tolerance estimation of steer-by-wire system under different resolver faults based on sensor flows," *Control Engineering Practice*, vol. 147, no. 105941, 2024.

[17] A. Balachandran and J. C. Gerdes, "Designing steering feel for steer-by-wire vehicles using objective measures," *IEEE/ASME Transactions on Mechatronics*, vol. 20, no. 1, pp. 373-383, 2015.

[18] Y. Liu, G. Zhang, J. Li, *et al*., "Steering feedback torque prediction based on sequence-to-sequence network with switcher-assisted training algorithm," *IEEE Transactions on Industrial Informatics*, vol. 20, no. 3, pp. 4894-4905, 2024.

[19] K. T. R. Van Ende, D. Schaare, J. Kaste, F. Küçükay, R. Henze, and F. K. Kallmeyer, "Practicability study on the suitability of artificial, neural networks for the approximation of unknown steering torques: Vehicle system dynamics," *Vehicle System Dynamic,* vol. 54, no. 10, pp. 1362–1383, 2016.

[20] R. Zhao, W. Deng, B. Ren, and J. Ding, "Modeling on steering feedback torque based on data-driven method," *IEEE/ASME Transactions on Mechatronics*, vol. 27, no. 5, pp. 2775-2785, 2022.

[21] S. Abbas, S. Husain, S. Al-Wais, and A. Humaidi, "Adaptive integral sliding mode controller (SMC) design for vehicle steer-by-wire system," *SAE International Journal of Vehicle Dynamic, Stability, and NVH,* vol. 8, no. 3, pp. 383-396, 2024.

[22] J. Lee, K. Yi, D. Lee, B. Jang, M. Kim, and S. Hwang, "Haptic control of steer-by-wire systems for tracking of target steering feedback torque," *Proceedings of the Institution of Mechanical Engineers, Part D: Journal of Automobile Engineering*, vol. 23, no. 5, pp. 1389–1401, 2020.

[23] Y. Liu, X. Wang, G. Zhang, Q. Yuan, Z. Chen, and L. Li, "Road sense construction for steer-by-wire system: data-driven feedback torque design and friction compensated explicit model predictive control," *IEEE Transactions on Transportation Electrification*, vol. 10, no. 4, pp. 9918-9930, 2024.

[24] S.-W. Oh, H.-C. Chae, S.-C. Yun, and C.-S. Han, "The design of a controller for the steer-by-wire system," *JSME International Journal Series C Mechanical Systems, Machine Elements and Manufacturing*, vol. 47, no. 3, pp. 896–907, 2004.

[25] S. Fankem and S. Müller, "A new model to compute the desired steering torque for steer-by-wire vehicles and driving simulators," *Vehicle System Dynamic*, vol. 52, no. 1, pp. 251–271, 2014.

[26] S. Achyuthan and N. K. Prakash, "Modelling of a steer-by-wire system with force feedback and active steering," in *2017 International Conference on Intelligent Computing and Control Systems (ICICCS)*, Madurai, India. 2017. pp. 676-680.

[27] J. Wang, H. Wang, C. Jiang, Z. Cao, Z. Man, and L. Chen, "Steering feel design for steer-by-wire system on electric vehicles," in *2019 Chinese Control Conference (CCC)*, Guangzhou, China, 2019, pp. 533-538.

[28] G. Zhu, H. Yang, and F. Yu, "Controller design for an automobile steer-by-wire system," in *2019 IEEE 28th International Symposium on Industrial Electronics (ISIE)*, Vancouver, BC, Canada. 2019. pp. 1492-1497.

[29] D. Cheon, C. Lee, S. Oh, and K. Nam, "Description of steering feel in steer-by-wire system using series elastic actuator," in 2019 *IEEE Vehicle Power and Propulsion Conference (VPPC),* Hanoi, Vietnam, 2019, pp. 1-4.

[30] M. Damian, B. Shyrokau, X. Carrera Akutain, and R. Happee, "Experimental validation of torque-based control for realistic handwheel haptics in driving simulators," *IEEE Transactions on Vehicular Technology*, vol. 71, no. 1, pp. 196-209, 2021.

[31] J. Jayachandran and D. Ashok, "Neural network-based approach for the generation of road feel in a steer-by-wire system," *Engineering Journal*, vol. 20, no. 5, pp. 49–66, 2016.

[32] J. Lee, S. Chang, K. Kim, *et al.*, "Steering wheel torque control of steer-by-wire system for steering feel," *SAE Technical Paper* 2017-01-1567, 2017.

[33] Z. Yang, G. Li, H. He, and G. Li, "Study on road feeling simulation control algorithm for four-wheel independent drive and steering electric vehicle," in *2017 Chinese Automation Congress (CAC)*, Jinan, China. 2017, pp. 4872-4875.

[34] R. A. Nikhil, S. Muhammed, and K. Nafeesa, "A new control strategy for improving steering feel of an EPAS system," in *2020 International Conference on Futuristic Technologies in Control Systems & Renewable Energy (ICFCR)*. Malappuram, India. 2020, pp. 1-6.

[35] Liuhe, X. Zeng, and L. Shuo, "Design of road feel feedback algorithm for steer-by-wire," in *2020 4th CAA International Conference on Vehicular Control and Intelligence (CVCI)*, Hangzhou, China, 2020, pp. 142-146.

[36] S. Woo, C. Heo, M.-O. Jeong, and J.-M. Lee, "Integral analysis of a vehicle and electric power steering logic for improving steering feel performance," *Applied Sciences*, vol. *13*, no. 20, pp. 11598. 2023.

[37] A. Alex and A. Saleem, "Artificial steering feel in steer by wire systems: a simulation-based evaluation of control strategies," in *2024 1st International Conference on Trends in Engineering Systems and Technologies (ICTEST)*, Kochi, India, 2024, pp. 1-8.

[38] A. Alex and A. Saleem, "A lyapunov-based dual controller approach with PSO tuning for steer-by-wire systems with artificial steering feel," *IEEE Access*, vol. 12, pp. 188976-188992, 2024.

[39] D. Fu, J. Feng, B. Wang, and Q. Liu, "Research on road sense simulation of steer-by-wire system," in *2023 5th International Academic Exchange Conference on Science and Technology Innovation (IAECST)*, Guangzhou, China, 2023, pp. 851-854.

[40] G. Shi, T. Liu, S. Wang, C. Guo, and Y. Liu, "High authenticity steering feel control strategy for Steer-by-Wire system based on terminal sliding mode rack force observer," *Proceedings of the Institution of Mechanical Engineers, Part D: Journal of Automobile Engineering*, vol. 0, no. 0, 2024.

[41] H. Zhou, A. Pang, J. Yang, and Z. He, "Structured H∞ control of an electric power steering system," *Complexity*, vol. 2020, no. 1, 2020.

[42] F. Heinrich, J. Kaste, S.G. Kabil, *et al.*, "Methods for modeling the steering wheel torque of a steer-by-wire vehicle," *Automotive and Engine Technology*, vol. 7, no. 1–2, pp. 53–64, 2022.

[43] S. C. Zou and W. Z. Zhao, "Synchronization and stability control of dual-motor intelligent steer-by-wire vehicle," *Mechanical Systems and Signal Processing*, vol. 145, pp. 106925, 2020.

[44] J. Tian, G. Tan, X. Pan, M. Cai, C. Huang, and Y. Yan, "Research on road sense simulation and stability control of SBW system," in *2021 China Automation Congress (CAC) 2021*, Beijing, China, 2021, pp. 4065–4070.

[45] H. Hwang, H. Choi, and K. Nam, "Practical synchronous steering angle control of a dual-motor driving steer-by-wire system," *IEEE Access*, vol. 7, pp. 133100–133110, 2019.

[46] L. De Novellis, A. Sorniotti, P. Gruber, and A. Pennycott, "Comparison of feedback control techniques for torque-vectoring control of fully electric vehicles," *IEEE Transactions on Vehicular Technology*, vol. 63, no. 8, pp. 3612–3623, 2014.

[47] S. S. Husain, M. Q. Kadhim, A. S. M. Al-Obaidi, A. F. Hasan, A. J. Humaidi, and D. N. Al Husaeni, "Design of robust control for vehicle steer-by-wire system," *Indonesian Journal of Science and Technology*, vol. 8, no. 2, pp. 197–216, 2023.

[48] D. Cheon, K. Nam, and S. Oh, "Design and robust control of a precise torque controllable steering module for steer-by-wire systems," *IEEE Transactions on Industrial Electronics*, vol. 69, no. 12, pp. 13245–13254, 2022.

[49] R. P. Borase, D. K. Maghade, S. Y. Sondkar, *et al.*, "A review of PID control, tuning methods and applications," *International Journal of Dynamic Control*, vol. 9, pp. 818–827, 2021.

[50] S. B. Joseph, E. G. Dada, A. Abidemi, D. O. Oyewola, and B. M. Khammas, "Metaheuristic algorithms for PID controller parameters tuning: review, approaches and open problems," *Heliyon*, vol. 8, no. 5, p. e09399, 2022.

[51] H. Khodadadi and H. Ghadiri, "Self-tuning PID controller design using fuzzy logic for half car active suspension system," *International Journal of Dynamic and Control*, vol. 6, pp. 224–232, 2018.

[52] B. Kristiansson and B. Lennartson, "Robust and optimal tuning of PI and PID controllers," *IEE Proceedings Control Theory Application*, vol. 149, no. 1, pp. 17–25, 2002.

[53] K. Ranjbaran and M. Tabatabaei, "Fractional order [PI], [PD] and [PI][PD] controller design using Bode's integrals," *International Journal of Dynamics and Control*, vol. 6, no. 1, pp. 200–212, 2018.

[54] M. R. Bongulwar and B. M. Patre, "Design of FOPID controller for fractional-order plants with experimental verification," *International Journal of Dynamics and Control*, vol. 6, no. 1, pp. 213–223, 2018.

[55] M. Lazar and W. Heemels, "Predictive control of hybrid systems: input-to-state stability results for sub-optimal solutions," *Automatica*, vol. 45, pp. 180–185, 2009.

[56] A. Cruz-Bernal, "Meta-heuristic optimization techniques and its applications in robotics," *Recent Advances on Meta-Heuristics and Their Application to Real Scenarios*, InTech, p. 53, 2013.

[57] J. Annisa, I. Z. M. Darus, M. O. Tokhi, and S. Mohamaddan, "Implementation of PID based controller tuned by evolutionary algorithm for double link flexible robotic manipulator," in *2018 International Conference on Computational Approach in Smart Systems Design and Applications (ICASSDA)*, Sarawak, Malaysia, 2018, pp. 1–5.

[58] M. A. Şen and M. Kalyoncu, "Optimal tuning of PID controller using Grey Wolf Optimizer algorithm for quadruped robot," *Balkan Journal of Electrical and Computer Engineering*, vol. 6, no. 1, pp. 29–35, 2018.

[59] D. Sandoval, I. Soto, and P. Adasme, "Control of direct current motor using ant colony optimization," in *2015 CHILEAN Conference on Electrical, Electronics Engineering, Information and Communication Technologies (CHILECON)*, Santiago, Chile, 2015, pp. 79–82.

[60] M. A. Azizul, F. Ahmad, J. Karjanto, M. H. Che Hasan, and S. Sulaiman, "Modelling, simulation and testing of steer-by-wire system with variable steering ratio control strategy in 14-DOF full vehicle model," *International Journal of Automotive and Mechanical Engineering*, vol. 21, no. 4, pp. 11784-11808, 2024.

[61] Y. Shengbing, D. Chunan, J. Xuewu, and C. Kuiyuan, "Research on road feeling control strategy of steer-by-wire," *SAE Technical Paper*, no. 2007-01-3652, 2007.

[62] H. Zheng, C. Zong, and L. Yu, "Road feel feedback design for vehicle steer-by-wire via electric power steering," *SAE Technical Paper*, no. 2013-01-2898, 2013.

[63] W. Liang, W. Zhao, C. Wang, and S. Zou, "Harmonic suppression and road feeling control of steer-by-wire system with permanent magnet synchronous motor," *Mechanical Systems and Signal Processing*, vol. 172, no. 108983, 2022.

[64] A. Kirli and M. S. Arslan, "Online optimized hysteresis-based steering feel model for steer-by-wire systems," *Advances in Mechanical Engineering*, vol. 8, no. 7, 2016.

[65] N. Bajçinca, R. Cortesão, and M. Hauschild, "Robust control for steer-by-wire vehicles," *Autonomous Robot*, vol. 19, pp. 193–214, 2005.

[66] H. Wang, H. Kong, Z. Man, D. M. Tuan, Z. Cao, and W. Shen, "Sliding mode control for steer-by-wire systems with AC motors in road vehicles," *IEEE Transactions on Industrial Electronics*, vol. 61, no. 3, pp. 1596-1611, 2014.

[67] Z. Sun, J. Zheng, Z. Man, and H. Wang, "Robust control of a vehicle steer-by-wire system using adaptive sliding mode," *IEEE Transactions on Industrial Electronics*, vol. 63, no. 4, pp. 2251-2262, 2016.

[68] D. Lee, K.-s. Kim and M. Han, "Model-based analysis of the hysteresis curve of an electric power steering system," in *2020 20th International Conference on Control, Automation and Systems (ICCAS)*, Busan, Korea (South), 2020, pp. 490-495.

[69] M. Selçuk Arslan, "A hysteresis-based steering feel model for steer-by-wire systems," *Mathematical Problems in Engineering*, vol. 2017, no. 2313529, 2017.

[70] M. Irmer, R. Degen, A. Nüßgen, K. Thomas, H. Henrichfreise, and M. Ruschitzka, "Development and analysis of a detail model for steer-by-wire systems," *IEEE Access*, vol. 11, pp. 7229-7236, 2023.

[71] A. Verl and T. Engelberth, "Adaptive preloading for rack-and-pinion drive systems," *CIRP Annals*, vol. 67, no. 1, pp. 369–372, 2018.

[72] D. E. Williams, "Synthetic torque feedback to improve heavy vehicle drivability," *Proc. Inst. Mech. Eng., Part D: J. Automobile Eng.*, vol. 223, no. 12, pp. 1517–1527, 2009.

[73] D. Williams and K. Sherwin, "Artificial steering feel," *SAE International Journal of Passenger Cars – Mechanical System*, vol. 2, no. 1, pp. 229–238, 2009.

[74] Y. Jiang, W. Deng, S. Zhang, *et al.,* "Studies on influencing factors of driver steering torque feedback," *SAE Technical Paper* 2015-01-1498, 2015.

[75] I. Kushiro and K. Suzuki, "Analysis for vehicle dynamics and steering system parameters effect on steering characteristics of steering feel (Fundamental study for performance design of objective target on steering feel)," *Transition JSME*, vol. 83, 2017.

[76] B.-H. Nguyen and J.-H. Ryu, "Direct current measurement-based steer-by-wire systems for realistic driving feeling," in *2009 IEEE International Symposium on Industrial Electronics,* Seoul, Korea (South), 2009, pp. 1023-1028.

[77] T. Dogruer and N. Tan, "Design of PI controller using optimization method in fractional order control systems," *IFAC-PapersOnLine*, vol. 51, no. 4, pp. 841–846, 2018.

[78] O. A. Somefun, K. Akingbade, and F. Dahunsi, "The dilemma of PID tuning," *Annual Reviews in Control*, vol. 52, pp. 65-74, 2021.

[79] A. R. Kumar and P. J. Ramadge, "DiffLoop: Tuning PID controllers by differentiating through the feedback loop," in *2021 55th Annual Conference on Information Sciences and Systems (CISS)*, Baltimore, MD, USA, 2021, pp. 1-6.

[80] D. W. Clarke, "Pretuning and adaptation of PI controllers," *IEE Proceedings - Control Theory and Applications*, vol. 150, no. 6, 2003.

[81] J. -W. Jung, V. Q. Leu, T. D. Do, E.-K. Kim and H. H. Choi, "Adaptive PID speed control design for permanent magnet synchronous motor drives," *IEEE Transactions on Power Electronics*, vol. 30, no. 2, pp. 900-908, 2015.

[82] J. Viola, L. Angel and J. M. Sebastian, "Design and robust performance evaluation of a fractional order PID controller applied to a DC motor," *IEEE/CAA Journal of Automatica Sinica*, vol. 4, no. 2, pp. 304-314, 2017.

[83] J. Qiao, Z. Liu, and Y. Zhang, "Gain scheduling based PID control approaches for path tracking and fault tolerant control of a quad-rotor UAV," *International Journal of Mechanical Engineering and Robotics Research*, vol. 7, no. 4, pp. 401–408, 2018.

[84] L. He, F. Li, C. Guo, B. Gao, J. Lu, and Q. Shi, "An adaptive PI controller by particle swarm optimization for angle tracking of steer-by-wire," *IEEE/ASME Transactions on Mechatronics*, vol. 27, no. 5, pp. 3830-3840, 2022.

[85] H. Choi and S. Choi, "Design of the steering feedback controller of a steer-by-wire system using admittance model," *International Journal of Automotive Technology*, vol. 25, pp. 565–574, 2024.

[86] H. Zhang, W. Jiang, W. Zhao, *et al.*, "Tracking and fault-tolerant controller design for uncertain steer-by-wire systems using model predictive control," *Chinese Journal of Mechanical Engineering*, vol. 37, p. 141, 2024.

[87] Y. Han, L. He, X. Wang, and C. Zong, "Research on torque ratio based on the steering wheel torque characteristic for steer-by-wire system," *Journal of Applied Mathematics*, vol. 2014, no. 929164, 2014.

[88] D. Karimi and D. Mann, "Torque feedback on the steering wheel of agricultural vehicles," *Computers and Electronics in Agriculture*, vol. 65, no. 1, pp. 77-84, 2009.

[89] R. C. Chabaan, "Torque estimation in electrical power steering systems," in *2009 IEEE Vehicle Power and Propulsion Conference*, Dearborn, MI, USA, 2009, pp. 790-797.

APPENDICES

Appendix A

Table A-1. 14-DOF model symbols

Symbols	Description
M_b	Mass of the vehicle
M_w	Mass of the tire
$\ddot{Z}_b$	Vertical acceleration of vehicle body
$\ddot{Z}_{w_i}$	Vertical acceleration of tire
F_{s_i}	Spring force at tire i-th position
F_{sfl}, F_{sfr}, F_{srl}, F_{srr}	Spring force acting on the front left, front right, rear left and rear right of the tire
F_{d_i}	Damper force at tire i-th position
F_{dfl},F_{dfr}, F_{drl},F_{drr}	Damper force acting on the front left, front right, rear left and rear right of the tire
F_{t_i}	Dynamic tire force at tire i-th position
K_{si}	Suspension spring stiffness at tire i-th position
C_{di}	Suspension damper coefficient at tire i-th position
K_{ti}	Spring stiffness of tire at i-th position
Z_{wi}	Sprung mass of vertical displacement at tire i-th position
Z_{bi}	Unsprung mass of vertical displacement at tire i-th position
$\dot{Z}_{wi}$	Sprung mass of vertical velocity at tire i-th position
$\dot{Z}_{bi}$	Unsprung mass of vertical velocity at tire i-th position
Z_{ri}	Road profile at tire i-th position
I_θ	Rotational inertia for the pitch axis
I_φ	Rotational inertia for the roll axis
I_γ	Rotational inertia for the yaw axis
$\ddot{\theta}$	Pitch acceleration
$\ddot{\varphi}$	Roll acceleration
$\ddot{\gamma}$	Yaw acceleration
b	Length from the center of vehicle gravity to the rear end of the vehicle
a	Length from the center of vehicle gravity to the front end of the vehicle
t	Length of the wheel track
F_{xfl},F_{xfr},F_{xrl},F_{xrr}	Longitudinal force at the front left, front right, rear left and rear right of the tire
F_{yfl},F_{yfr},F_{yrl},F_{yrr}	Lateral force at the front left, front right, rear left and rear right of the tire
δ	Steer angle of tire
$F_{z,fi}$, $F_{z,ri}$	Normal forces for front or rear tires (left or right side)
g	Gravitational acceleration
a_x	Longitudinal acceleration
l	Wheelbase of vehicle
H_{CG}	Length from the center of gravity to the bottom of the vehicle
α_{fi}	Lateral slip angle of tire for front tires (left or right side)
α_{ri}	Lateral slip angle of tire for rear tires (left or right side)
v_x	Longitudinal vehicle velocity
v_y	Lateral vehicle velocity
$\dot{r}$	Yaw rate
δ_f	Steer angle of front tire
$\sigma_{f/r}$	Lateral slip angles of front and rear tire
$v_{tiref/r}$	Velocity of the front and rear tire
$\omega_{f/r}$	Angular velocity of the front or rear tire
R_w	Tire radius

Table A-1. (cont.)

Symbols	Description
$v_{xf/r}$	Longitudinal velocity component of the front or rear tire
I_{ω}	Inertia of the tire
$\ddot{\omega}_{fi}$, $\ddot{\omega}_{ri}$	Angular velocity of the front or rear tire (left or right side)
T_{dfi}	Driving torque of front tire (left or right side)
T_{bfi}, T_{bri}	Applied braking torque at front or rear tire (left or right side)
$T_{trac.fi}$,$T_{trac.ri}$	Traction torque at front or rear tire (left or right side)

Appendix B

Table B-1. Steering wheel model parameters and corresponding values

Parameters	Description	Value
I_{sw}	Equivalent moment of inertia at steering wheel	-
B_{sc}	Viscous damping of the steering wheel	= 0.136 Nms/rad
K_{S1}	Lumped short-column compliance	= 3500 Nm/rad
$T_{fr,c}$	Equivalent torque friction at steering wheel	= 2 Nm
T_{driver}	Torque input from driver	-
I_{m1}	Rotational inertia of shaft motor 1	= 1 kgm^2
T_{m1}	Torque motor 1	-
θ_{sw}	Steering wheel's angular displacement	-
$\dot{\theta}_{sw}$	Steering wheel's angular velocity	-
$\ddot{\theta}_{sw}$	Steering wheel's angular acceleration	-
B_{m1}	Viscous damping of the shaft motor 1	-
θ_{m1}	Angular displacement of motor 1	-
$\dot{\theta}_{m1}$	Angular velocity of motor 1	-
$\ddot{\theta}_{m1}$	Angular acceleration of motor 1	-
V_{S1}	Voltage source to motor 1	-
$V_{inductor}$	Voltage across the inductor	-
$V_{motor\ resistance}$	Voltage across the motor resistance	-
V_{emf}	Electromotive force voltage at motor 1	-
L_1	Inductance motor 1	= 0.002 H
R_1	Resistance motor 1	= 4.6 ohm
k_e	Electromotive force constant	= 0.35 Vs/rad
i_{a1}	Current motor 1	-
$\frac{di_{a1}}{dt}$	Current rate motor 1	-

Table B-2. Front wheel model parameters and corresponding values

Parameter	Description	Value
M_{rack}	Mass of the rack	= 2.0 kg
y_{rack_y}	Lateral displacement of the rack	-
$\dot{y}_{rack_y}$	Lateral velocity of the rack	-
$\ddot{y}_{rack_y}$	Lateral acceleration of the rack	-
K_{Lf}	Steering linkage stiffness	= 26000 Nms/rad
K_{s2}	Lumped torque sensor stiffness	= 3500 Nms/rad
r_L	Offset of the king pin axis	= 0.3 m
r_P	Pinion gear radius	= 0.035 m
$F_{fr,rack_f}$	Rack friction	= 9 Nm
B_{rack_f}	Damping coefficient of the rack	= 1.032 Nms/rad
B_{kpf}	King pin damping coefficient	= 30 Nms/rad
$T_{fr,kpf}$	Friction torque around the king pin axis	= 2 Nm
R_2	Resistance motor 2	= 0.6 ohm
L_2	Inductance motor 2	= 0.002 H
I_f	Rotational inertia of the wheel	= 270 kgm^2
I_{m2}	Rotational inertia of the motor shaft	= 1.9 kgm^2
M_z	Wheel alignment moment	-
B_{m2}	Viscous damping of the motor shaft	= 1 Nms/rad
T_{m2}	Torque motor 2	-
θ_{m2}	Angular displacement of motor 2	-
$\dot{\theta}_{m2}$	Angular velocity of motor 2	-
$\ddot{\theta}_{m2}$	Angular acceleration of motor 2	-
δ_F	Actual front wheel steer angle	-
$\dot{\delta}_F$	Actual front wheel angular velocity	-
$\ddot{\delta}_F$	Actual front wheel angular acceleration	-

Appendix C

Table C-1. Parameter of vehicle model

Parameter	Description	Value
M_b	Mass of vehicle	= 833 kg
t	Track width	= 1.415 m
l	Wheelbase	= 2.35 m
a	Distance front axle to CG	= 1.1 m
b	Distance rear axle to CG	= 1.25 m
C_{df}	Suspension damping constant front	= 1.032
C_{dr}	Suspension damping constant rear	= 1.032
A	Frontal area of vehicle	= 1.6 m^3
M_w	Mass of wheel	= 20.75 kg
K_{sf}	Suspension spring stiffness front	= 18000 N/m
K_{sr}	Suspension spring stiffness rear	= 18000 N/m
H	Distance from ground to CG	= 0.54 m
I_φ	Moment of roll	= 270 kgm^2
I_θ	Moment of pitch	= 750 kgm^2
I_γ	Moment of yaw	= 750 kgm^2
R_w	Tire radius	= 0.27 m
g	Gravitational acceleration	= 9.81 m^2